Review

The frontier of tungsten oxide nanostructures in electronic applications

Siqi Zhou,[1] Zanhe Yang,[1] Xiangyu Feng,[1] Jiaxin Zuo,[1] Nannan Wang,[1,*] Kunyapat Thummavichai,[2,*] and Yanqiu Zhu[1,*]

SUMMARY

Electrochromic (EC) glazing has garnered significant attention recently as a crucial solution for enhancing energy efficiency in future construction and automotive sectors. EC glazing could significantly reduce the energy usage of buildings compared to traditional blinds and glazing. Despite their commercial availability, several challenges remain, including issues with switching time, leakage of electrolytes, production costs, etc. Consequently, these areas demand more attention and further studies. Among inorganic-based EC materials, tungsten oxide nanostructures are essential due to its outstanding advantages such as low voltage demand, high coloration coefficient, large optical modulation range, and stability. This review will summarize the principal design and mechanism of EC device fabrication. It will highlight the current gaps in understanding the mechanism of EC theory, discuss the progress in material development for EC glazing, including various solutions for improving EC materials, and finally, introduce the latest advancements in photo-EC devices that integrate photovoltaic and EC technologies.

INTRODUCTION

Introduction

In the current era of increasing severe environmental challenges, the emissions of carbon dioxide (CO_2) in human production and life are still high, with over 3.6 billion tons of CO_2 emitted annually from the combination of fossil fuels, execution production, and other social construction and development processes.[1] Considering the risks posed by emerging industries, it is most likely that the construction industry, contributing to 37% of global CO_2 emissions, is the largest consumer of energy.[2] Replacing traditional technologies with new environmentally friendly technologies—i.e. energy-saving glass—is one way to reduce pollution emissions in the building construction.[3] This intelligent energy-saving glass, known for its ability to drastically cut energy consumption, has the unique ability to dynamically adjust light transmission properties on demand,[4] providing greater control over the amount of light and heat entering the building.

Operating on the principle of electrochromic (EC) device inherent in metal oxides, the advent of smart windows has revolutionized building energy efficiency and indoor comfort.[5] When the self-controlled voltage is applied, the luminous flux of visible light changes, resulting in macroscopic adjustments in color or opacity. The sun's heat energy is transmitted to the building through thermal radiation, which often increases the need for indoor air condition due to the absorption of unnecessary heat energy. However, smart windows, with their ability to adjust discoloration and opacity can effectively reduce solar energy solar intake. This not only minimizes the energy required for indoor air conditioning but also prevents the absorption of unnecessary heat, thereby contributing to overall energy efficiency.[3,6]

First concept of EC was introduced by Platt in 1961. Subsequently, in 1969, Deb demonstrated the unique capability of tungsten oxide (WO_x) to achieve reversible coloring, either through ultraviolet light irradiation or an external potential. ED refers to the phenomenon in which various organic and inorganic materials produce new or different visible bands when redox reactions occur due to change in their redox states and electronic absorption bands.[7] Since the discovery of electrochromism and its advantages in terms of rich color, energy saving, environmental protection, and intelligent control, EC technology has led to its application in various fields including intelligent windows, intelligent displays, anti-dazzle mirrors, and so on (Figures 1A–1F).[10–20]

An EC device is operated similarly to a thin-film battery. The reaction process involves the transfer of electrons from electroactive substances (i.e., donors and receptors of electrons in redox reaction) on electroactive films.[21] EC materials can reversibly change the light absorption properties within a certain wavelength range. This is achieved by attaching two materials, one in a complete bleaching state and the other in a complete coloring state, to both ends of the electrode. The reversible color change is then realized through oxidation and reduction,[22,23] composed of a multi-layer structure that includes an EC material, electrolyte, and ion storage layer (Figure 2). Two transparent conductive electrodes sandwiched between these layers required two redox pairs each. The material with the highest coloring rate is attached to the

[1]State Key Laboratory of Featured Metal Materials and Life-cycle Safety for Composite Structures, MOE Key Laboratory of New Processing Technology for Nonferrous Metals and Materials, School of Resources, Environment and Materials, Guangxi University, Nanning 530004, China
[2]Department of Mathematics, Physics and Electrical Engineering, Faculty of Engineering and Environment, Northumbria University, Newcastle-upon-Tyne NE1 8ST, UK
*Correspondence: wangnannan@gxu.edu.cn (N.W.), kunyapat.thummavichai@northumbria.ac.uk (K.T.), y.zhu@gxu.edu.cn (Y.Z.)
https://doi.org/10.1016/j.isci.2024.109535
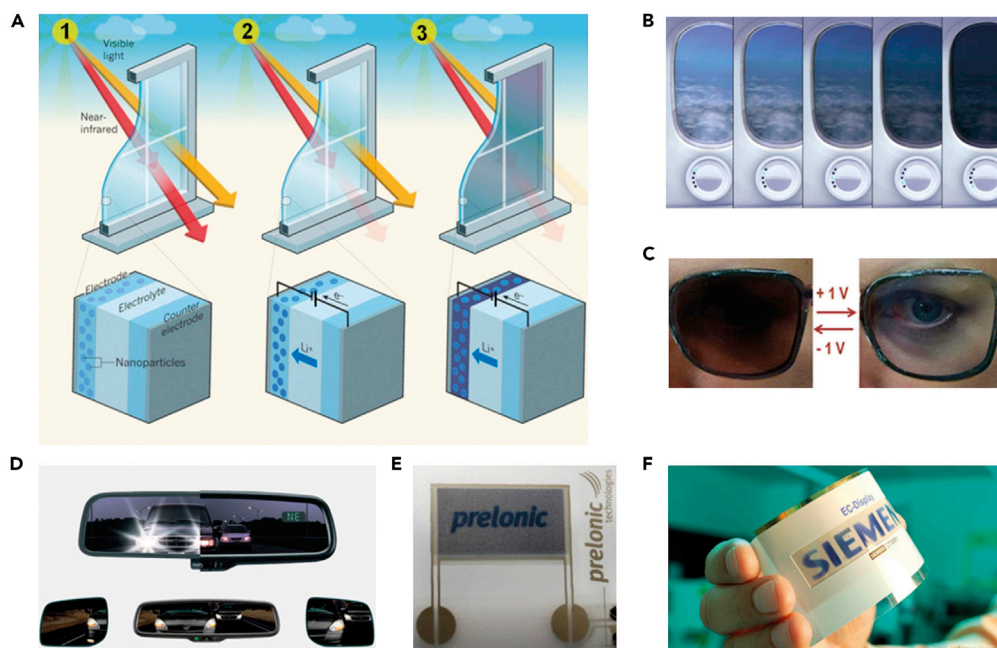
Figure 1. Applications of electrochromic devices

(A) Design of electrochromic window. Reprinted with permission ref.[8] Copyright 2013, Macmillan Publishers.

(B) Smart switchable window applied in Boeing aircraft produced by SmartTintW.

(C) Photographs of the electrochromic lens. Reprinted with permission from ref.[9] Copyright 2015, American Chemical Society.

(D) Automatic dimming mirror based on electrochromism produced by Gentex. Printable and flexible electrochromic displays designed by (E) Prelonic Technologies and (F) Siemens. Copyright©2023 Elsevier B.V. or its licensors or contributors. ScienceDirect is a registered trademark of Elsevier B.V.

working electrode and the ion storage material without EC activity is used as another simple counter electrode, and the color is changed through external potential charge and discharge.[25] At the center of EC device structure is ion conductors which are responsible for conducting electricity. The ion conductor layer in EC devices is very similar to the ion conduction reaction in batteries. They are all related to faradaic reactions. When the faradaic reactions occur in ion migration, the electrode material will undergo reversible coloring, that is, electrochromism.[26]

Despite the advent of smart windows, they continue to grapple with several challenges such as long response time, material degradation, installation cost, etc. In response to these challenges, researchers have been focusing on the development of device design and EC materials. Particularly, EC materials based on the transition metal oxides have seen significant advancements. Scientists have proposed many methods to improve the properties of these EC materials. These include forming composite materials through the doping metals, organics and inorganics, or downsizing the material to create nanoscale transition metal oxides. Such modifications have proven effective in improving the stability, color adjustment, and opacity of EC materials.[27,28]

In addition, under ideal conditions, the ideal optical modulation of the EC material is 100%. Simply speaking, when the EC material is in the bleaching state and the coloring state, the material should correspond to the completely transparent state and the completely opaque state, respectively. However, most of the research groups or research teams are unable to verify that the optical modulation of EC materials is greater than 80%.[29–33] Obviously, there is still a big challenge for us to achieve 100% optical modulation of EC materials. So far, WO_x-based nanostructured films have shown porous and nanoscale interconnected network structures due to their ultra-high transmittance and WO_3 films prepared by short-interval pulse electrochemical deposition,[34] and WO_3 films can exhibit higher EC activity.[35] These characteristics make WO_x-based nanostructured films a strong competitor in the field of EC research.

This review aims to offer a comprehensive understanding of this exciting field and its potential for future development. The review delves into properties, applications, degradation, and regeneration of WO_x-based nanostructures within the realm of EC materials. We will also shed the latest advantages in research progress of WO_x-based nanostructures. Finally, we will provide an overview of the current progress, future trends, and challenges of the WO_x-based nanostructures and their electronic applications.

BASIC MORPHOLOGICAL AND STRUCTURAL FORMS OF WO_x STRUCTURE

WO_x itself is composed of a large number of polymorphs and sub-stoichiometry and has inherent oxygen vacancies (V_O) and tunnels in the energy band structure.[36] In general, from the existence of V_O in the lattice, WO_x crystals can be divided into two forms: stoichiometric tungsten oxide (WO_3) and non-stoichiometric tungsten oxide (WO_{3-x}). These oxides, known as the Magnéli phase, exhibit diverse properties depending on the specific composition of WO_x. For instance, when 3-x < 2.5, the WO_{3-x} films are conductive and metallic in appearance. Films
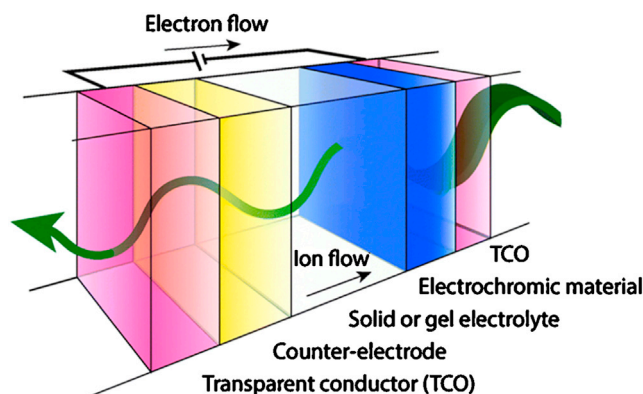
Figure 2. Schematic of the electrochromic device
Electrons flow through an external circuit into the electrochromic material, while ions flow through the electrolyte to compensate the electronic charge. Reprinted with permission from ref.[24] Copyright 2014, Royal Society of Chemistry.

with 3-x = 2.7–2.5 appear blue and conductive. On the other hand, films with 3-x > 2.7 are transparent and have resistance.[37] The crystal model of WO_3 can be approximated by a ReO_3 cubic model.[38] However, due to various internal defects, WO_{3-x} exhibits different crystal structures at different temperature ranges. For example, it forms a tetragonal crystal system above 740°C, an orthogonal crystal system between 330°C and 740°C, a monoclinic crystal system between 17°C and 330°C, and a triclinic system between 50°C and 17°C, and so on. Different crystal structures can lead to different material properties of WO_x. For an example, hexagonal WO_3 shows fast response in EC performance (5/6 s for coloration/bleaching) and significant optical modulation (78.1%)[39]; these advantages are attributed to the ordered ion channels in the hexagonal crystal structure.[40]

The color of WO_x can also vary depending on their stoichiometry. For example, WO_3 is general yellow or light green in color. The presence of gaps and V_O in sub-stoichiometric and stoichiometric films can help explain the differences in optical and EC properties between different films.[41] For example, the EC behavior observed in amorphous WO_3 films is mainly attributed to small polarized molecular transitions and F-like color centers. On the other hand, the coloring mechanism in crystalline WO_x film is Drude-like free electron absorption, which behaves similarly to heavily doped semiconductors with ionized impurities.[42]

Compared to their microsize, WO_x nanoparticles demonstrate enhanced EC performance, and this performance is further improved with a reduction in particle size.[43] One-dimensional (1D) nanostructures of WO_3 come in various forms including nanowires, nanotubes, nanofibers, nanorods, and nanobelts. Meanwhile, two-dimensional (2D) WO_3 has been acknowledged as a stable crystalline phase, largely due to its high specific surface area compared to its 1D structures. We have made this point more clear in the study of Zhao et al.[44] They prepared 2D-WO_3 nanonetworks by thermal evaporation, and clearly found by scanning electron microscopy that they are more fluffy and ultrafine than 1D-WO_3 nanomaterials, which also proves that 2D-WO_3 has a higher specific surface area. Thanks to the low-dimensional characteristics of 2D-WO_3, quantum confinement plays a significant role. This not only alters the electronic properties, but also enables the preproduction of multi-form nanomaterials, such as disks-like nanostructure and thin sheets.[45] The presence of V_O inside structure can determine whether WO_3 can be condensed into a 2D structure, known as crystal shear plane. If the V_O content exceeds the limit, the WO_6 octahedron transforms from a common angle connection to a common edge connection, resulting in a WO_3 plate that is separated by the defect area (crystal shear plane). The generation of high valence tungsten is attributed to the excess V_O, which also improves the conductivity of the material.[46]

From a thermodynamic perspective, WO_3 is more stable than WO_2 as indicated by their formative enthalpies: WO_3 has a ΔHF, 298 of -201.46 kcal mol^{-1}, while WO_2 has a ΔHf:298 of -140.94 kcal mol^{-1}, WO_2 crystallizes in twisted rutile, which can be observed through the edge-sharing WO_6 octahedron.[47] As mentioned earlier, the structure of WO_3 may originate from cubic ReO_3 structure. However, in addition to this structure, WO_3 can also occur in a metastable hexagonal modification.[48]

In terms of the electronic structure of WO_3, stoichiometric WO_3 is a wide band-gap semiconductor (i.e., 2.5–3.2 eV[49–54]), and the width of the band gap depends on the structure. Numerous studies have investigated the electronic characteristics of WO_3, with the recent findings showing that the Kohn–Sham's band gap of monoclinic phase at room temperature is 3.13 eV, while the band gap of cubic phase is 1.89 eV.[55,56]

WO_x has a very complex and flexible electronic structure, rooted in its basic octahedral unit (WO_6). This unit can undergo various permutations and combinations, forming new crystal structure through the sharing of angles, edges, and faces. The nanostructures of WO_x play critical role in its performance, as nanosized materials with different morphologies exhibit unexpected behaviors. The various morphology of WO_x including nanoparticles, nanosheets, nanorods, ultra-thin films, and more has injected strong vitality into the field of advanced nanotechnology materials.

PREPARATION METHODS OF NANOSTRUCTURED TUNGSTEN OXIDE

In today's advanced development environment of nanomaterials, reducing the size and dimension of oxides has become an important research requirement. WO_x nanoparticles with high crystalline structure have a higher solubility in acidic solutions than ordinary crystals, which

limits their use in practical applications. Therefore, there is need to optimize the existing preparation methods and improve the size control of WO_x nanomaterials to address this contradiction.[57,58] Various methods are employed to synthesize nanostructured WO_x such as the sol-gel method, the solvothermal synthesis method, the hydrothermal method, the template method, etc. Tungsten powder, tungsten chloride, and peroxy tungstic acid, etc., can serve as precursors for the preparation of 1D or 2D WO_x nanomaterials.[59]

It is important to note that the selected preparation method can significantly influence the size, structure, and properties of the resulting WO_x materials. The effective synthesis of WO_3 nanostructure is a key factor that greatly affects the performance of WO_x films.[60] In this section, we will explore primary methods for synthesizing nanostructured WO_x, highlighting their unique characteristics and roles in the production process.

The sol-gel method

The sol-gel method is a technique that offers a straightforward, efficient, and cost-effective means of preparing nanoparticles. It is widely used in the synthesis of nanocomposite and nanocrystals with complex structures offering the advantages of low processing temperatures and ease of use.[61] The sol-gel method involves several key steps including (1) hydrolysis, (2) polycondensation, (3) aging, (4) drying, and (5) thermal decomposition.[62]

This technique is based on the hydrolysis and polycondensation of precursor molecules, which can be performed under mild reaction conditions (heat and stir in a water bath at 85°C for 8–12 h to obtain a slightly yellow and transparent sol).[63] In the review by Badilescu et al., two chemical methods for forming solid-phase chemical networks are detailed. The first method, known as the metal-organic route, involves adding metal alkoxides to organic solvents. For instance, tungsten alkoxide salts, which remain stable in anhydrous organic media, quickly react with water. This reaction leads to rapid hydrolysis followed by dehydration or dealcoholization, resulting in the formation of an inorganic polymerization network. The second method, termed the inorganic route, incorporates metal salts such as chlorides, nitrates, and sulfides into an aqueous solution. Unlike the metal-organic route, which uses organic solvents, this method utilizes water-based reactions to achieve the chemical network.[64] Chai et al. studied the effect of aging time on the preparation of hydrated WO_x by sol-gel method. No structure could be detected on the first day of initial aging, but formed hydrated tungsten oxide platelets of 1-1.θ 3m after 30 days of aging, which can greatly increase the uniformity of water.[65,66]

The hydrothermal method

The hydrothermal method is a process to obtain the crystalline powder, coating, and single crystal directly in the liquid phase. The method requires relatively low-temperature conditions (i.e., add range of temperature a bit). In brief, the hydrothermal method involves using water as the solvent and dissolving and recrystallizing the powder. Recently, advancements in the hydrothermal preparation of nanoparticles have led to the development of several innovative techniques including supercritical hydrothermal route, continuous hydrothermal route, and hydrothermal modification route, each offering unique advantages in the synthesis process.[67]

Gao et al. found that using insoluble *p*-nitrobenzoic acid as a promoter in the hydrothermal process resulted in the formation of the defective WO_3 nanoplates with intermediate pores. The influence of hydrochloric acid on the final product was greatly reduced when the tungstic acid precursor was washed with water during the synthesis process. As a result, the synthesized nano-WO_3 exhibited high photocatalytic degradation of methylene blue.[68] Mohan et al. compared various synthesis methods of nano-WO_3 materials in recent studies including chemical vapor deposition, sputtering, laser ablation, sol-gel technology, microwave plasma, and hydrothermal synthesis. Their findings suggested that the hydrothermal synthesis of nano-WO_3 offered the greatest environmental protection coefficient, coupled with low cost and ease of operation.[69] Figure 3 shows the formation process of WO_3 nanocubes by hydrothermal synthesis.

In addition, Thummavichai et al. found that metal dopants can significantly improve the performance of EC materials prepared by hydrothermal method. They investigated the effects of niobium, gadolinium, and erbium doping on tungsten oxide using a single-step solvothermal technique. Their research results show that controlling the content and size of metal dopants is a key way to improve the excellent EC performance materials obtained by hydrothermal method. Through the data provided by them, we found that compared with pure WO_x, low doping concentration leads to distorted structure, which helps Li^+ insertion/deinsertion to obtain better EC performance.[71]

The solvothermal synthesis method

Choi et al. used a simple process to produce nano-WO_x. Tungsten hexachloride was used as a precursor and dissolved in a proportionate mix of ethanol and water. The well-mixture was then subjected to solvothermal treatment at 200°C. After 10 h, $W_{18}O_{49}$ and WO_3 nanoparticles were obtained (Figure 4). Interestingly, they found that alteration in the concentration of the precursor materials significantly influenced the morphology of the final product.[72]

The template method

Employing the template method can yield nanomaterials with high crystallinity and specific surface area, thereby enhancing their performance in catalytic reactions. The approach also facilitates the integration of nanomaterial synthesis and assembly, addressing the issue of nanomaterials dispersion stability. High crystallinity can reduce the recombination of electron-hole pairs, while high specific surface area can increase the density of active surface sites where catalytic reactions can occur.[73]
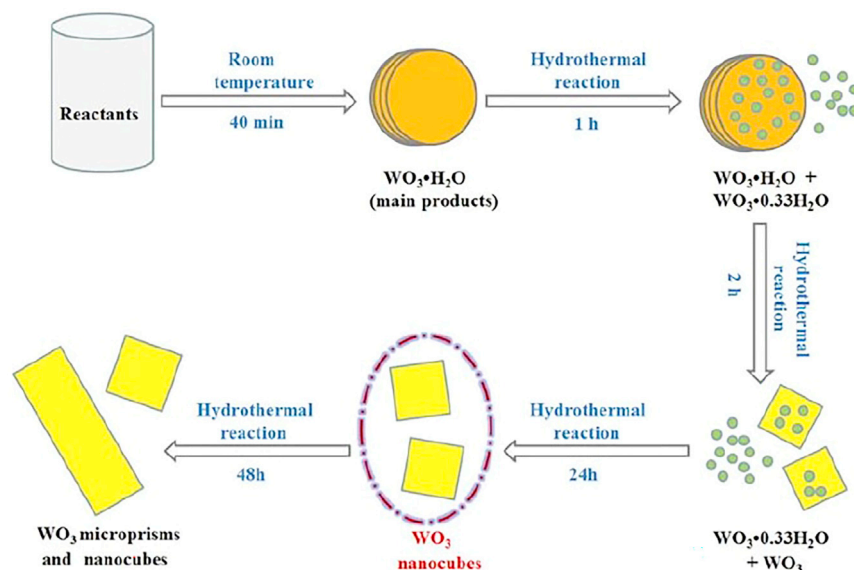
Figure 3. Schematic illustration of the formation of WO$_3$ nanocubes via hydrothermal synthesis
Reprinted with permission from ref.[70] Copyright © The Authors, published by EDP Sciences, 2021.

For WO$_3$ nanofilm materials used in the EC reaction, the template method involves depositing controllable nanostructure materials into the holes of the template by physical or chemical methods. Once the template is removed, materials with the desired shape can be obtained. This method allows for production of nanomaterials with standardized morphology and size. Essentially, the template method is a process that involves creating templates based on hydrothermal method, which ultimately leads to the production of nanomaterials.[74]

Generally, templates are categorized into two groups, namely hard and soft templates, according to their structural differences.[75,76] A hard template (e.g., NaCl,[77] CaCO$_3$,[78] etc.) is a rigid material with stable structure that can directly determine the size and morphology of sample particles. On the other hand, the soft template such as mesoporous alumina enriched with lanthana,[79] etc., does not have a fixed structure, and does not appear as a rigid material.[75] After the synthesis of nanomaterials via the template method, the final, crucial step involves the removal of the template (i.e., dissolution, sintering, and etching methods, etc.). This step is of paramount importance as it can significantly influence the physical and chemical properties of the resulting product.[80] According to Hongo's work, the hard template method is a powerful
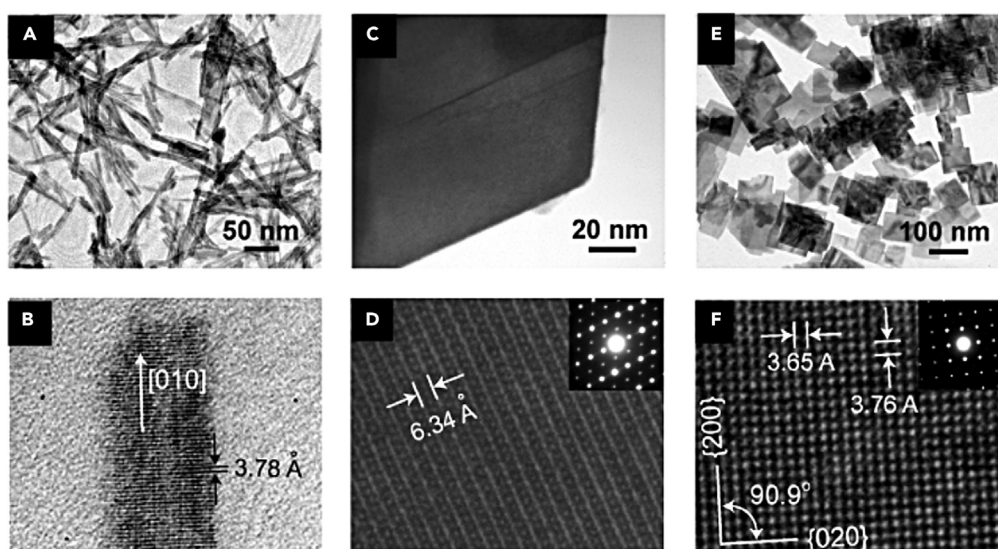
Figure 4. TEM images of tungsten oxide particles
TEM images (top) and corresponding high-resolution atomic images (bottom) of tungsten oxide particles: (A), (B) sample ES, monoclinic W$_{18}$O$_{49}$; (C), (D) sample MS, hexagonal WO$_3$; and (E), (F) sample WS, monoclinic WO$_3$. Reprinted with permission from ref.[72] Copyright © 2023 The American Ceramic Society, all rights reserved.
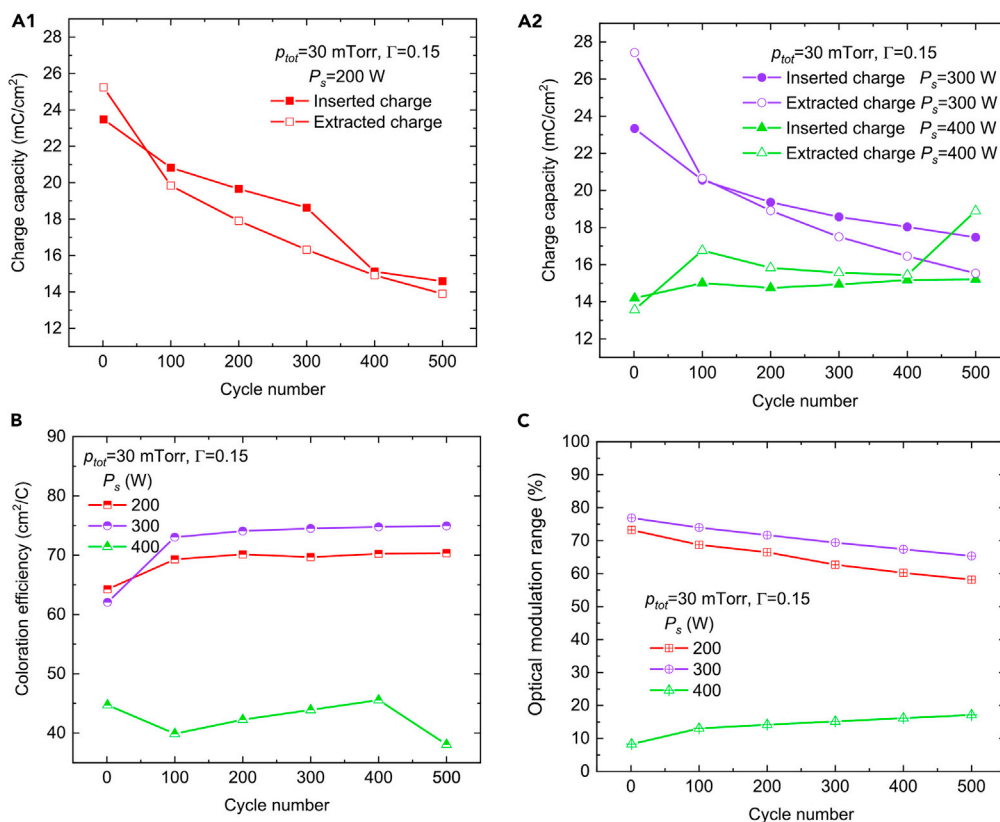
Figure 5. The EC properties of WO$_x$ films prepared by DC magnetron sputtering

(A1 and A2) Capacity of inserted and extracted charge, (B) coloration efficiency, and (C) optical modulation range for ~300 nm-thick films of W oxide prepared by sputtering at the shown values of O$_2$/Ar gas flow ratio in the sputter plasma Γ, total pressure of the sputter plasma ptot, and sputtering power Ps. Data were taken for different values of Ps during continuous voltammetric cycling in an electrolyte of LiClO$_4$ in PC at a voltage scan rate of 20 mV/s. Measured data are indicated by symbols which are joined by straight lines for clarity. Data for Ps = 200 W were shown in Figure 4 and but are included here to allow easy assessment on the role of Ps. Reprinted with permission from ref.[83] Copyright © 2023 Elsevier B.V. or its licensors or contributors.

and effective method for production of nanostructured crystals. Utilizing this method, they synthesized nanostructured WO$_3$ from sheet mesoporous silica SBA-15. The result was an ordered nanorod array that inherited the hexagonal p6mm structure with boasting a BET surface area value of 30m^2/G. This arrayed WO$_3$ comprise two crystalline phases, specifically tetragonal and monoclinic symmetries.

Other preparation techniques

Enhancement of the production method of WO$_x$ nanomaterials can boost their application efficiency. The traditional methods for preparing nano-WO$_x$ (i.e., sol-gel, hydrothermal, and template methods[81,82]) lack the ability to controlling the crystal size. An alternative method for synthesizing nanoparticles with controllable size, morphology, and crystallinity is flame spraying technology. In this route, Hidayat et al. utilized larger sub-micron particles as precursors for preparing nanomaterials via this method, which provides significant advantages in reducing material costs, operation difficulty, and time.[43]

Atak et al. used DC magnetron sputtering (with 5 cm diameter w target) to prepare WO$_x$ thin films which were then analyzed for their EC performance via lithium perchlorate (LiClO$_4$) electrolyte in propylene carbonate potentiostat system. They found that selecting more appropriate deposition parameters can greatly improve the cycle durability of WO$_x$ thin films under repeated voltage. This study reveals an excellent improved method for preparing WO$_x$ films with good cycle durability.[83] Figure 5 summarizes their experimental results.

DC magnetron sputtering technology, which involves the acceleration of atoms by electrons under an electric field, is utilized in the fabrication of EC material films, and is particularly suitable for creating metal-WO$_x$. The procedure involves the use of plasma composed of oxygen and argon in the reactive magnetron sputtering process. This approach is generally preferred in the production of EC smart glass. Such a technical scheme can meet the requirements of producing materials with sufficient EC properties and excellent deposition rates over large area, up to a few square meters.[84–87]

Deshpande et al. synthesized high-density WO$_x$ nanoparticle crystals using hot filament chemical vapor deposition (HWCVD), and doped these particles into the EC film which greatly improved the device's EC performance.[88] In brief, chemical vapor deposition is a type of chemical vapor deposition method where a filament is heated to a high temperature, causing a chemical reaction that results in the deposition of material
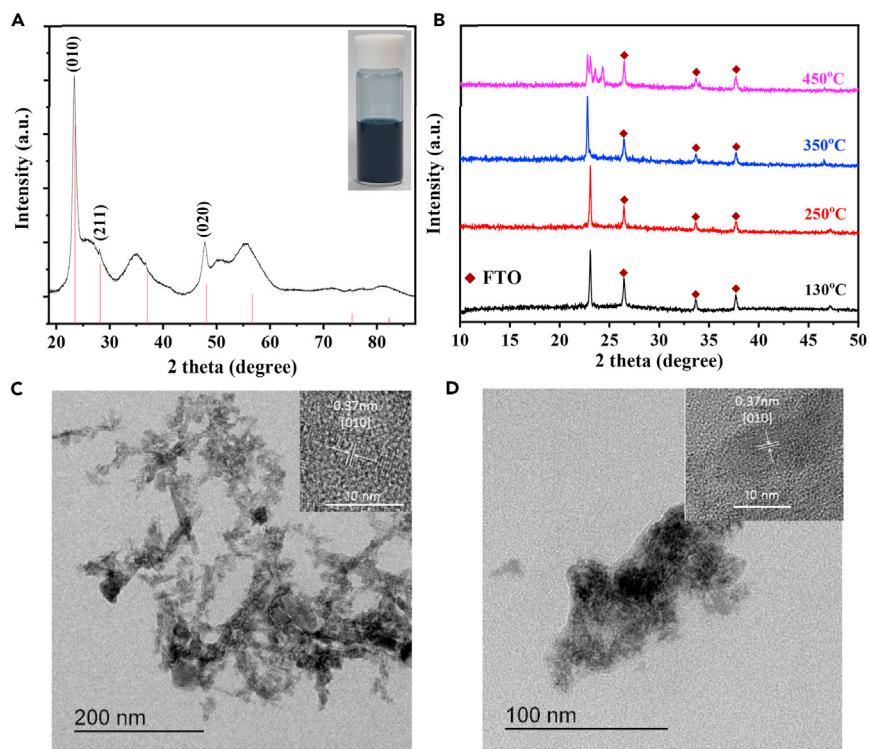
Figure 6. The XRD pattern of the solvothermally synthesized WO$_{3-x}$ powder

(A) XRD pattern (black line) of the synthesized WO$_{3-x}$ powder. Red lines corresponding to XRD pattern of the W$_{18}$O$_{49}$ (jcpds No. 64–0773) – the insert shows the dark blue color of the synthesized WO$_{3-x}$ solution in ethanol ($\sim$10 mg mL $-$ 1), (B) XRD pattern of the WO$_{3-x}$ films annealed at 130°C, 250°C, 350°C, and 450°C, and TEM/HR-TEM (insert) images of (C) the near WO$_{3-x}$ powder and (D) the 250 W sample (for interpretation of the references to color in this figure legend, the reader is referred to the web version of this article.). Reprinted with permission from ref.[90] Copyright©2022 The Author(s). Published by Elsevier B.V.

onto a substrate. Deshpande et al. first created a static atmosphere of argon and oxygen, and placed a single tungsten wire in it, randomly heated to 1400° C (measured by optical high-temperature determination), and the oxygen concentration was maintained between 5% and 16% during this experimental change. All depositions were carried out at 150 Torr reactor pressure and 300°C furnace temperature. After about 20 min, the material is deposited on the wall of the reactor. The crystalline phase of nanoparticles can be customized by changing the HWCVD synthesis parameters[89]; the optimal synthesis conditions occur when an O$_2$ partial pressure of $\sim$4% is employed in an Ar ambient with Pch = 150 Torr. The synthesis temperature is maintained at 300°C with an external furnace, and the tungsten filament is operated at 1400°C. The cycle durability in an acid electrolyte (3,000 cycles) can be greatly improved by doping nano-sized WO$_3$ into the film, while other films can only complete 500 cycles.[58]

Park et al. studied the dual-band of anoxic WO$_x$-based EC window which can effectively control infrared and visible light independently and dynamically. The anoxic WO$_x$ nanoparticles were prepared via the basic solvothermal method. To improve the dispersion of nanoparticles in the solvent used for thin film deposition at lower temperatures, they also designed the oil ink coating method with high dispersion under the mixing of various solvents. Through the use of X-ray diffraction, high-resolution transmission electron microscopy, and *in situ* spectroelectrochemical measurement, it was found that oxygen-deficient level of WO$_x$ can independently and dynamically control the transmittance of infrared and visible light under the annealing condition of 350°C (Figure 6).[90]

Nanocrystalline WO$_3$ film, mesoporous WO$_3$ film, and layered WO$_3$ hollow shell are considered to have better optical effects than WO$_3$ bulk.[91–93] This has been confirmed by Kim's team who synthesized WO$_3$ with different diameters using the dense micro-WO$_3$ layer and the porous nano-WO$_3$ layer. They prepared EC batteries by nanoparticle deposition system, a method they believe could replace the expensive and environmentally problematic sol-gel and sputtering methods.[94] The results showed the insertion of a large amount of Li+ ions with a 90% transmittance change of 30 s for micro-WO$_3$ and 26 s for nano-WO$_3$. When the volume percentage of micron WO$_3$ and nano-porous WO$_3$ is 9:1, 5:5, and 1:9, the switching times were recorded as 21, 25, and 18 s, respectively.[95–97]

Similarly, Song's team reported the development of a layered mesoporous silica microsphere/WO$_3$ nanocrystalline hybrid film (THMS/WO$_3$) doped with Ti (as shown in Figure 7). They explored its EC properties and found that after 100 coloration and bleaching cycles, the THMS/WO$_3$ film maintained its dark blue color in the coloring state, and was nearly transparent in the bleaching state.
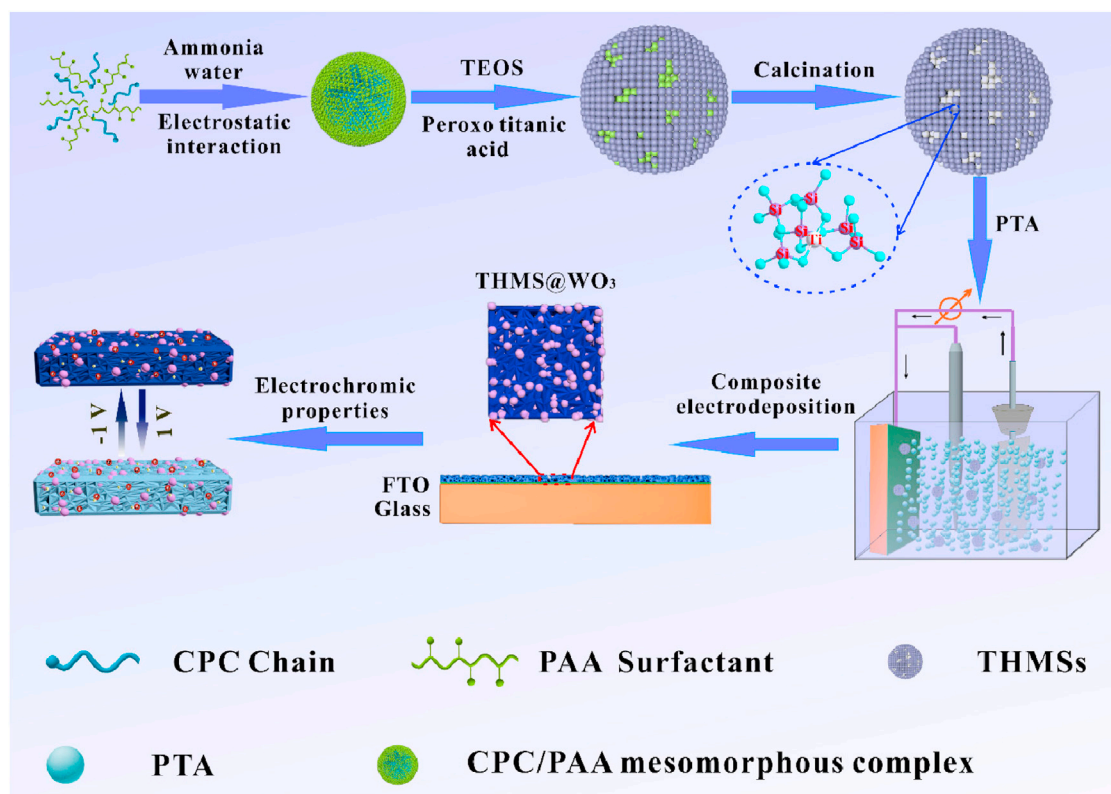
Figure 7. Schematic illustration of the fabrication and electrochromic property of the Ti-doped hierarchically mesoporous silica microspheres/tungsten oxide (THMS/WO₃) hybrid films

Reprinted with permission from ref.[98] Copyright©1996–2023 MDPI (Basel, Switzerland) unless otherwise stated.

OPTICAL PRINCIPLE OF MATERIALS AND THEIR ROLE IN EC APPLICATIONS

This section mainly delves into these two aspects, exploring how the internal structure of a material influences its transparency and how the absorption and re-emission of light contribute to a material's color. Furthermore, we will discuss the practical implications of these properties in the use of EC devices, highlighting the key parameters that indicate the quality of EC products.

The performance and functionality of EC materials, which are capable of changing their optical properties under an applied electric field, are largely determined by two key factors: the transparency of the materials and the effects of electro-redox reactions. In general, the transparency of the material is determined by the optical effect of the scattering and refraction of visible light waves, which are influenced by the material's internal structure. When the light enters the materials, multiple scattering and refraction occur. If the scattering degree is weak or virtually non-existent, the material shows such characteristics of transparency. Conversely, if the degree of scattering is intense, preventing light waves from passing through, the material is characterized as having low transparency or being opaque.[99]

There are numerous factors contributing to the internal scattering of materials. Generally, microcrystalline with anisotropic refractive index within the material is the primary cause of strong scattering. Due to the disordered orientation of these microcrystals, light will inevitably undergo multiple scattering and refraction at the adjacent interface, resulting in diffused light. Not only the microcrystalline structure of the material, but also the fine dispersion of two phases with different refractive indices can cause light scattering.[100] For example, while amorphous homogeneous polymers are generally transparent, crystalline polymers with both crystalline and amorphous regions tend to scatter significantly due to the differing refractive indices of those regions.[101] In addition, block copolymers, graft copolymers, and blend polymers are mostly two-phase systems, and thus, are generally translucent and opaque.[102,103]

The color of a material and its coloring principle are also crucial factors. The absorption of light by materials is indeed a process where the material's molecules absorb photons of a specific wavelength from the continuous spectrum, leading to the excitation of electrons and their subsequent transition. When the material is solid, the atoms that absorb the photons interact with each other, causing in a splitting of the energy level and a broadening of the emission line. This broadening also affects the absorption spectrum line, leading to a wider absorption region or even an absorption band on the optical wavelength distribution map.

In general, the light transmitted through a material is a composite wave, containing both non-absorbing and re-emitting light waves. Non-absorbing light wave originates from the portion of the incident light that the material does not absorb. On the other hand, the re-emission light wave arises from the excitation of the electrons. When electrons absorb photons, they are excited from their ground state to the excited state. These high energy, unstable excited electron will soon transition back to their stable ground state.[104] The single EC material, WO_x, can transition
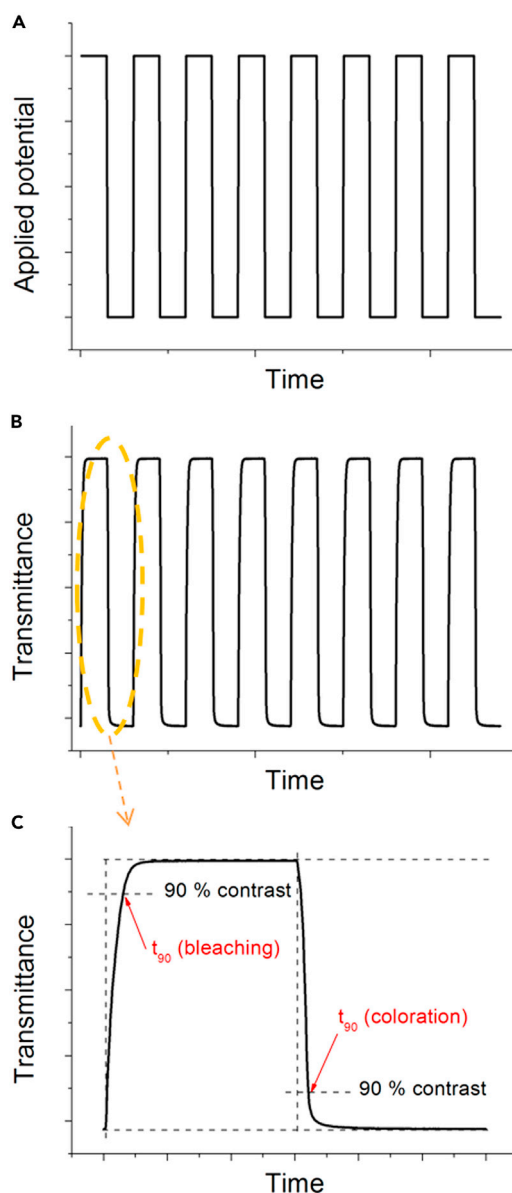
Figure 8. Conventional procedure for reporting switching times
(A) Square-wave potential steps with fixed pulse lengths.
(B) Corresponding transmittance evolution at a fixed wavelength.
(C) Switching time at an arbitrarily chosen percentage of a full switch (90% in this case), whether for bleaching or coloration. Reprinted with permission from ref.[111]
Copyright© 2018 Elsevier B.V. All rights reserved.

gradually from transparent to blue. This change is attributed to an increase in the transmittance of blue light, resulting from a decrease in the concentration of WO^+_{3-x} ions at the cathode. As a consequence, the material adopts a dark blue color in its colored state.[105,106]

The coloring effect is generally based on the interplay between the material inherent properties and various factors such as spectrum, brightness, hue, saturation, etc.[107,108] The intensity of the transmitted or reflected light determines the brightness, while the hue is determined by the dominant wavelength of the reflected or transmitted light. Meanwhile, the proportion of the dominant wavelength in the white light defines the saturation. When it comes to the practical use of the EC device, there are four key parameters that are used as benchmark to gauze the quality of the EC products.

(1) Optical contrast

The percentage change of absorbance and transmittance, which reflects the impact of EC color change, is a primary parameter considered in the practical application of EC device.[109] This parameter is crucial as it directly relates to the device's ability to modulate light and hence the
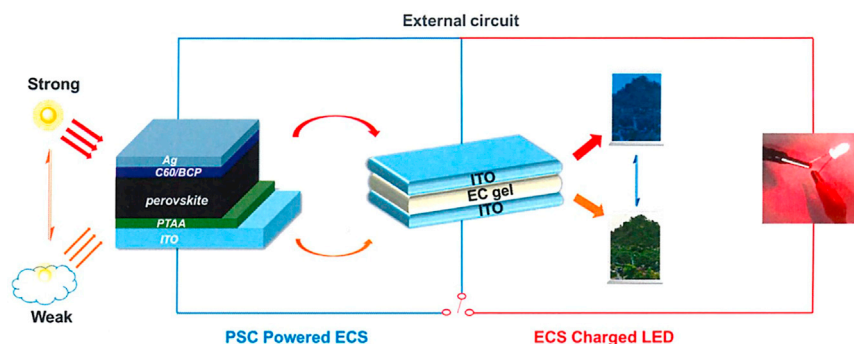
Figure 9. Perovskite solar cell (left) harvests solar energy to drive ECD (electrochromic devices)/ECS (electrochromic supercapacitors) to different colored states under different light intensities, and the stored energy of ECS (in deep colored state) can light a red LED (right)
Reprinted with permission from ref.[181]Copyright© 2023 Springer Nature Limited.

greater the percentage change in absorbance and transmittance, the more pronounced the color change, and the more effective the EC device is likely to be. This can be represented as following Equation 1.[110]

$$\Delta T = T_b - T_c \text{ or } \Delta A = A_C - A_b \qquad \text{(Equation 1)}$$

ΔT-transmittance; ΔA-absorbance; T_c, A_c-colored state; T_b, A_b-bleaching state

(2) Color switching time.

Typically, scientific literature reports a 90% or 95% switching time for the EC material to complete its full contrast switch.[26] This is due to the face that the change of light transmittance over time generally follows an exponential pattern making it difficult to pinpoint the exact moment of the transition. Thus, the focus is on the time it takes for material to achieve a significant majority of its total possible color change (i.e., 90%).

Hassab's team proposed an accurate formula for calculation of the switching time, which involves using symmetrical potential steps of varying pulse lengths to switch the device and monitor the change in transmittance at required wavelength. The contrast value obtained is then expressed as a function of the pulse length and fitted to the formula (Equation 2, Figure 8).[111]

$$\Delta T(t) = \Delta T_{max}\left(1 - e^{-\frac{t}{\tau}}\right) \qquad \text{(Equation 2)}$$

Where ΔT_{max} represents the full-switch contrast obtained for long pulse lengths and τ is the time constant.

(3) Coloration efficiency (CE)

The actual power consumption in the discoloration process is related to the efficiency of EC device color change at the same energy.[112]

$$\eta = \frac{\Delta OD}{Q_d} = \frac{\Delta A}{Q_d} = \frac{\log(T_b/T_C)}{Q_d} \qquad \text{(Equation 3)}$$

η-CE; Q_d-injection charging unit area; ΔA-absorbance; T_b, A_b-bleaching state

(4) Cycle stability

Cycle stability is a key parameter that reflects the maximum number of cycles the EC device can transition between the colored state and the bleached state, or vice versa. Similar to many electrical appliances, the cycle index determines the EC device lifespan. To ensure the longevity, EC devices are often sealed to protect against unfavorable factors such as moisture and other airborne substances that could shorten the device's lifespan.

MATERIAL SOLUTION IN EC DEVICES

Inorganic-based EC devices are mainly constructed from transition metal oxide materials (e.g., iridium, tungsten, cobalt, manganese, nickel, palladium, cerium, rhodium, ruthenium, titanium, and molybdenum oxides), such as antimony EC film, three-dimensional ordered macroporous vanadium oxide EC film, and nickel oxide-based EC thin film.[113–131] Among inorganic-based EC materials, WO_x offers better EC redox reaction effect, multi-color characteristics in reversible intercalation/deintercalation process, and fast switching response compared to other metal oxides. Moreover, WO_x is a non-toxic, light-stable n-type semiconductor with a band gap of about 2.6 eV, enabling it to absorb a wide range of visible light.[132–134] Currently, the most commercially viable products are generally based on WO_3 as the EC material substrate.[36,135,136] Materials with potential EC properties include inorganic materials, organic materials, inorganic-organic hybrid materials, and plasma materials, which are generally divided into two categories: organic and inorganic.[137–140] For most organic materials such as bipyridine chlorides, transition metal-ligand complexes, and conjugated polymers. Organic EC materials generally have the advantages of rich

color and easy processing.[141–146] WO$_3$ not only has broad application prospects in the field of electrochromism, but also has important research value in the fields of photocatalysis, thin film photothermal effect, gas sensitivity, supercapacitor, and so on.[147–154]

In the realm of EC materials, both organic and inorganic variants face their own unique challenges. Inorganic-based EC devices, typically constructed from transition metal oxide materials, grapple with material degradation issues that arise from ion insertion. On the flip side, organic EC devices, despite offering high flexibility and wearability, are hampered in their practical applications due to their poor durability under light working conditions.

Material degradation issue of WO$_3$ materials or thin film is characterized by a gradual reduction in optical modulation ability of EC device and increase in the response time, both of which are consequences of long-term charge insertion and extraction, leading to a decline in EC performance. When the ions enter the host structure and are subsequently extracted, some ions might fail to be successfully removed. Over time, this residual ion accumulation weakens the bleaching and coloring state of the WO$_3$ film. Furthermore, the ions that have not been successfully extracted from the structure will form an internal electric field inside the film, causing a resistance to subsequent coloring and bleaching process.[155,156]

Apart from material degradation issue, WO$_3$ EC materials have certain limitations including low ion transport efficiency and low conductivity compared to those of organic type. These drawbacks result in a lower coloring efficiency of EC device.[157] Addressing the low coloration efficiency of EC materials is a significant challenge. Future research efforts will likely focus on adapting EC devices to complex environments, whether through the development of new EC materials or other innovative approaches This will be a significant step toward improving the durability and efficiency of these devices.

Development of hybrid EC materials

It is well known that nanostructured WO$_x$ materials offer superior EC performance compared to their micro or bulk counterparts. To further enhance this, the EC performance of WO$_x$ based materials can also be improved through doping techniques These doping techniques, which include metal doping, organic doping, and inorganic doping, have been reported to significantly enhance the coloration efficiency of EC nanomaterials.[158–162] Wang's team prepared WO$_x$-titanium dioxide thin film composite on the ITO substrate.[163] The result shows that pure WO$_3$ film typically exhibits a blue hue within the visible light spectrum. The addition of TiO$_2$ into the composite glass results in a striking jewel blue color. This unique coloration offers promising potential for use in EC device or, smart glass that requires specific base color characteristics. Xu et al. reported the excellent characteristics of photothermal WO$_3$ film that uses an external electric field to cooperate with a three-dimensional porous WO$_3$ to further enhance photothermal conversion and sterility in the colored state. The principle behind this is that the film can tune the localized surface plasmon resonance of Au nanostructures and broadband non-radiative plasma decay. In the experiment, WO$_3$, Au nanoparticle-Au nanorod (Au PR)/WO$_3$, and Au nanoparticle (Au P)/WO$_3$ films were irradiated with 915 nm near-infrared for 300 s. After observing the survival rate of *E. coli* on the films, it was concluded that the survival rate of *E. coli* was affected by the photothermal effect of the film, which was independent of the voltage, and the AuPR/WO$_3$ film was a promising and effective antibacterial coating.[164]

Gu's team proposed a layer-by-layer self-assembly technology to conveniently integrate P$_8$W$_{48}$ and W$_{18}$O$_{49}$ nanocomposites materials that can absorb both visible and near-infrared light. This composite material has the ability to dynamically control the transmittance of both near-infrared (750–1360 nm) and visible light (400–750 nm) in a quick and reversible manner, simply by adjusting the potential.[165] Wang's team conducted a study using vanadium and tungsten as substrates to investigate the impact of film composition and thickness on the spectroelectrochemistry and EC characteristics of the films. They found notable effects when the ratio of vanadium to tungsten was 1:1 and the film's thickness was set at 110 nm. The amorphous vanadium WO$_x$ film demonstrated superior inertia and exceptional storage capacity. Furthermore, they noted that the device they fabricated exhibited a coloring time of 5 s and bleaching time of 1.7 s at 90 ΔT% in the 1,100 nm band. The cycle stability is up to 10,000 times. This shows ultra-fast response speed and excellent cycle stability, and has great development potential.[166]

An effective strategy to enhance EC devices could be achieved by combining the strengths of both inorganic and organic materials, aiming to leverage these distinct advantages, potentially overcoming the limitations such as material degradation in inorganic materials and poor light durability in organic materials. Shi et al. has proposed a promising approach to enhance the EC properties of WO$_3$ by integrating poly (3,4-ethylenedioxythiophene) (PEDOT) nanoshells with WO$_3$ nanocores. The PEDOT nanoshells provide flexibility and stability, while the WO$_3$ nanocores contribute to the desired EC functionality.[167] The result show that this hybrid structure offers an impressive coloring time of 3.8–12.4 s and bleaching time of 3.6–7.6 s. This depends on two reasons. On the one hand, the large contact area between the porous hybrid nanostructures and the electrolyte to load cations improves the accessibility of the electrolyte to the active sites of the hybrid nanostructures. On the other hand, WO$_3$ can interact with p-doped PEDOT as an electron acceptor to form an electron donor-acceptor pair, thereby improving the interaction between the inorganic/organic interface.[168] Coordination nanosheet (CONASH) is a kind of nanosheet composed of organic ligands with metal ions/atoms/clusters. Bera et al.'s WO$_3$-based CONASH nanosheets show excellent performance tests in EC durability. The results show that the material has a high EC life of at least 15,000 cycles.[169] This makes CONASH a promising material for the development of long-lasting EC device.

Hou et al. conducted a study on tantalum (Ta) and WO$_x$ doped with conjugated polymer composite materials. The team studied a fully solution-processed double-layer porous extraction contact consisting of Ta-WO$_x$ and polythiophene derivative poly [5,5′-bis (2-butyl) -(2,2′-bithiophene) 4,4′-dicarboxylic acid-substitutive-5,5′ −2,2′-bithiophene]. The Ta-WO$_x$ interface layer allows a significant reduction in the transport barrier between the electrode and the p-conjugated polymer.[170]

The Dinca team used matrix-assisted pulsed laser evaporation technology to form a controllable EC composite interface.[171] Cyclic voltammetry measurements showed that the WO_3 electrode exhibited a typical cathode peak at −0.2 V and a typical anode peak at 0 V. And the cathode peak of GO/WO_3 composite appears at −0.25 V, and the cathode peak of GO/WO_3 composite appears at −1.9 V. This indicates that the layer-by-layer film has a lower reduction potential than the film obtained from the mixture. In fact, this is supported by the fact that the cathode peak of the GO/WO_3 mixture shifts to a more negative value, indicating that the reduction of WO_3 at this interface is more difficult. Khan et al. prepared (WO_3/rGO) composite films by a simple hydrothermal method. The composite film exhibits a high CE value of 181.5 cm^2/C at the wavelength of 633 nm, which is higher than that of WO_3 film (CE = 122.2 cm^2/C). In addition, these films also show good cycle stability maintaining performance up to 2,500 cycles. They suggested that the interface between rGO and WO_3 could be the main reason for enhancing of the electron transfer efficiency of the material.[172]

In summary, both nanocrystallization and doping present effective methods for enhancing the performance of tungsten oxide-based EC materials. Often, these two methods are used in conjunction, or organic and inorganic doping are applied sequentially. By adjusting the ratio of different raw materials used in doping and the degree of nanocrystallization, it is possible to optimize the conditions for producing high-performance products.

Development of flexible EC device

Currently, a growing damage for flexible EC device that suitable for certain application (i.e., wearable technology, flexible display, and other innovation applications). Therefore, developing flexible EC device that can maintain high performance and durability remains a challenge. The use of ITO materials for EC device comes with certain limitations. For example, Li's team reported that ITO struggles to withstand repeated bending, and the scarcity and rapid depletion of indium make it less suitable for creating low-cost flexible devices.[173] To overcome these challenges, Li's team developed WO_3/Ag/WO_3 (WAW)-laminated films. This film can serve not only as transparent electrodes but also as EC materials. Moreover, the material can be prepared at room temperature, non-toxic and low cost. Compared to WO_3 monolayer films, these WAW films exhibit superior EC optical properties, including high transmittance (480%), long-term cycle stability (3,000 times), and short switching time (i.e., 11 s for coloration, and 10.5 s for bleaching).[174] Lin et al. synthesized $WTi_xO_yC_z$ organic-doped thin films with flexible properties, similar to those of WAW.[175] The results showed that the film could be bent around a rod with a diameter of 2.5 cm for 1,000 times without any degradation. It is worth mentioning that the porous surface of $WTi_xO_yC_z$ film has a high grain boundary fraction of 19.5%. After 200 cycles of Li^+ intercalation and deintercalation, the film exhibited a significant light modulation of 82.7%, and the coloring efficiency of 71.2 cm^2/C at 850 nm. They also demonstrated excellent switching times, offering a switching efficiency of 31 s for coloring and a swift 5 s for bleaching. This impressive performance is attributed to the high grain boundary fraction on the porous surface of the $WTi_xO_yC_z$ film. This structure enables the reversible embedding and de-embedding of Li^+ ions with less resistance, thereby enhancing the overall efficiency of the EC process.

ADVANCEMENTS IN EC TECHNOLOGY: A FUSION WITH INNOVATIVE ENERGY SOLUTIONS

Enhancing energy efficiency through the reduction of energy consumption and the recycling of energy can significantly alleviate these problems. EC devices are instrument in this process as they facilitate substantial energy saving through efficient energy conversion and storage.[176] These devices primarily absorb light in the wavelength range of visible light within the modulated solar spectrum. Nearly 50% of the energy in the solar spectrum is located in the near-infrared band, indicating that EC device mainly focuses on the absorption of visible light and near-infrared waves.[177] By achieving independent control of visible light and near-infrared radiation light could allow flexible adjustment of sunlight and heat entering the building.[5,178]

In recent years, the practical applications of inorganic EC materials have demonstrated significant commercial value. As a result, the utilization rate of inorganic EC materials has substantially exceeded that of organic EC materials.[179] Inorganic materials are mainly divided into transition metal oxides and ferricyanide $Fe_4[Fe(CN)_6]$ 3-based systems. Inorganic EC materials generally have the advantages of good material durability, wide working range, and high chemical stability.[180] Transition metal oxides are promising EC materials with good flexibility, mainly including WO_3, TiO_2, Nb_2O_5, MoO_3, and so on.

One of the advantages of EC devices is that the conditions for light absorption only require a small driving voltage. However, if it is insensitive to light molecules or unstable absorption, this advantage of EC devices will be seriously affected. Huan et al. invented an integrated gel EC device powered by perovskite solar cells, which can adjust the absorption of light by automatically switching between bleaching and coloring states. It can be used for 70,000 cycles, and the power conversion efficiency can be maintained at 18.3%, showing excellent chemical stability. The experimental data show that this integrated perovskite EC device is expected to become the framework of energy storage intelligent window, which lays a foundation for the realization of all-weather intelligent window (Figure 9).[181]

Spinel $Li_4Ti_5O_{12}$ (LTO) is an ideal anode material for lithium batteries and can be used as a raw material for rechargeable EC energy storage devices (EESDs). In the experiment, the LTO film exhibits excellent theoretical capacitance and structural stability. In addition to the advantages of these two most EC capacitors, LTO also exhibits good optical contrast during energy storage and conversion. It can effectively block 90% of the thermal radiation energy in sunlight in the wavelength range of visible light and near-infrared light. This rechargeable EESD can be used as an architecture for modern smart windows, providing a way to promote energy recovery.[182] The birth of EC supercapacitor devices has also promoted the invention of smart windows and energy-saving applications. A self-charging EC supercapacitor device (SC-ESCD) for a sliding-mode DC triboelectric nanogenerator has excellent electrochemical performance and stable cycle performance. When the current is 0.1 mA cm^{-2}, SC-ESCD has a capacitance of up to 15.2 mF cm^{-2}. After 5,000 cycles, the capacitance only decreased by 1%, which confirmed

that SC-ESCD had excellent stability. The discovery of SC-ESCD also provides a direction for creating a self-charging power supply that integrates energy collection, storage, and electrochromism.[183]

ADVANCEMENTS IN WO$_x$ UTILIZATION FOR DIVERSE APPLICATIONS

There are many active sites on the surface of the nanostructure, which can effectively shorten the ion transfer path and increase the motion rate, thereby improving the switching speed.[184,185] As an inorganic transition metal oxide, WO$_x$-based nanostructures discussed in the following section usually produce cathode coloring by simultaneous injection of electrons and ions under cathode bias.[5] It has now become a popular choice in modern EC materials.

In the TeO$_2$-B$_2$O$_3$ glass system, WO$_3$ was doped into the composite using melt-spinning method. It was observed that as the concentration of WO$_3$ increased and the molar volume expanded, the density and refractive index of the glass samples decreased from 5.4794 to 3.3579 g/cm^3 and from 2.628 to 2.522 g/cm^3, respectively. This indicates a negative correlation between the WO$_3$ concentration and the density as well as the refractive index of the glass samples. The glass sample obtained from the TeO$_2$-B$_2$O$_3$ system doped with WO$_3$ exhibits an amorphous microstructure. The direct optical band gap varies from 2.37 to 3.12 eV, and the indirect optical band gap varies from 2.27 to 2.58 eV. This can be concluded that the doping of WO$_3$ did not significantly improve the radiation shielding ability of the glass system, but it showed an increase in the band gap and a decrease in the refractive index, which may have favorable competition conditions in applications such as graded index fiber.[186]

Almuqrin et al. found that the TeO$_2$-WO$_3$ glass system doped with Bi$_2$O$_3$ and PbO can also shield radiation to a certain extent.[187] Lithium bismuth borotungstate glasses with chemical composition of 20Li$_2$O-(20-x) Bi$_2$O$_3$-xWO$_3$-60B$_2$O$_3$ (x = 0, 1, 2, 3, 4, and 5 mol %) were prepared using quenching method. The addition of high crosslinking density of WO$_3$ into the glass composition results in the reducing of non-bridging oxygen and free volume within the glass. Moreover, the inclusion of WO$_3$ modifies the direct and indirect band gaps of the glass, making the glass structure more stable and harder. Hence, the microhardness of the glass samples reaches 4.98 GPa, showing an increase of 0.16 GPa compared to the undoped glass. Stalin et al. found that this bismuth lithium borotungstate glass can be used in high-energy radiation occasions such as nuclear research structures, has stable chemical properties, and can shield gamma rays.[188]

By self-assembly of phosphoric acid protective layer on the top of WO$_3$ electrode, the electrochemical corrosion of WO$_3$ electrode is hindered, the electrolyte limitation is overcome, and the stability of the electrode is improved. The self-assembled molecular layer provides hydrophobicity, significantly increasing the cycle life of the WO$_3$ electrode. The wrapped WO$_3$ electrode can undergo more than ten times the number of cycles compared to an unprotected electrode in the 1 M KCl electrolyte system. Even after more than 1,000 cycles, the WO$_3$ electrode can maintain a maximum current density of 60%. Hopmann et al. proved that the self-assembled monolayer modification of WO$_x$-based materials enhances the cycle life of EC devices, particularly in harsh electrolyte environments.[189]

The activity of EC properties can be improved by embedding metal nanofiber array (NFA) into WO$_3$ bifunctional electrode. With the NFA embedded, this WO$_3$-based nanocomposite effectively prevents charge transfer resistance and improves the electrochemical activity of active molecules at the electrode-electrolyte interface, thus exhibiting excellent stability, coloring efficiency, and light modulation ability. Even after 2,000 cycles, the performance remains stable. Figure 10 illustrates the formation of the NFA on the WO$_3$ electrode film and presents experimental data corresponding to the excellent properties of this composite material. The NFA-embedded WO$_3$ electrode also enhances electrochemical energy storage activity and exhibits excellent performance as an intelligent supercapacitor.[190]

Chen et al. designed a double-sided EC device by imitating the differential coloring of the dorsal (anterior) side and ventral (posterior) side of the wings with reference to some butterfly species in nature, such as Nymphalidae. Through different driving voltages, the two sides will exhibit significantly different coloring states due to the thin metal layer with complex refractive index. (Fabrication of dual Z-scheme TiO$_2$-WO$_3$-CeO$_2$-heterostructured nanocomposite with enhanced photocatalysis, antibacterial, and electrochemical performance). A special device is called Janus structure EC device. The optical modulation layer in the device is often composed of absorbing metals such as W, Cu, Ti, or Ag, and the initial color asymmetry on both sides can be controlled by the thickness of W, WO$_3$, and indium-doped tin oxide layers. Chen et al. believed that this asymmetric EC will be extended to the infrared spectrum, that is, thermal radiation, and as a new type of EC device, it can broaden the application scenarios.[191] Chang et al. studied an EC device using WO$_3$ as a material by electroexplosive wire technology, and controlled the size distribution of WO$_3$ nanomaterials in deionized water by changing the explosion voltage.[192] Wang et al. combined solvothermal method and calcination method to prepare a 3D WO$_{3-x}$ EC supercapacitor, and studied the optical and electrochemical properties of the dual-function electrode nanowire networks/fluorine-doped tin oxide (NWNs/FTO). The experimental results show that the WO$_{3-x}$ NWNs/FTO cathode has an area specific capacity of up to 57.57 mF cm^{-2} and an optical modulation of up to 85.05%. After 10,000 cycles, the specific capacitance rate can still be maintained at 87.53%, and the homologous optical modulation range is maintained at 75.42%, which is considered to have stable cycle performance (Figure 11).[193]

OUTLOOK AND SUMMARY

In recent times, there have been numerous breakthroughs in the study of EC tungsten oxide, leading to the development and utilization of various new hybrid nanomaterials and EC materials. While the advantages of WO$_x$ have been extensively explored and recognized, its potential for future development remains substantial. However, it is important to acknowledge the limitation and challenges associated with its practical application and future research. These shortcomings primarily include the following aspects.
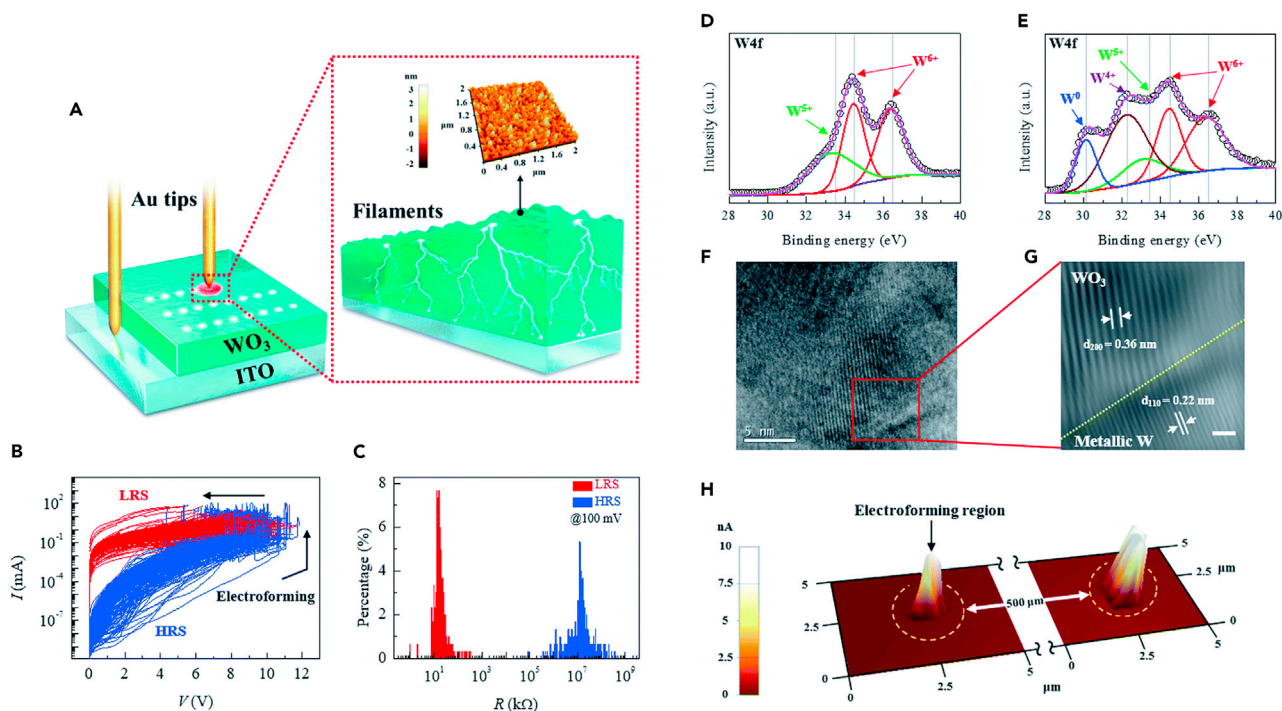
Figure 10. A metal oxide-based smart supercapacitor electrode by embedding a nanoscale metallic nanofilament array (NFA)

(A) Schematic showing the formation of a conducting nanofilament array (NFA) across a WO_3 electrode film via an electroforming process.

(B) Resistance-switching current–voltage (I–V) curves of the WO_3 film showing bi-stable resistance states.

(C) The resistance distribution of the low- and high-resistance states extracted at a 0.1 V read voltage. XPS spectra of (D) the pristine WO_3 and (E) NFA-embedded WO_3 films.

(F) Cross-sectional high-resolution TEM image of the NFA-embedded WO_3 film and (G) a magnified view showing the Moiré fringes.

(H) Conductive-AFM image of the NFA-embedded WO_3 electrode measured with a compliance current of 10 nA. Reprinted with permission from ref.[190] Copyright© Royal Society of Chemistry 2023.

(1) The development of nanoscale WO_x materials necessitates advancements in the control of size and refinement of preparation methods. As materials reach the quantum size regime, careful control of shape and size is essential to prevent significant reductions in performance. Traditional preparation methods of nanomaterials like sol gel method and hydrothermal method need enhancement to meet the higher structural and performance requirements of nanomaterials. For example, as a core EC material, WO_x faces the challenge of balancing cost and cycling resistance especially when applied as a nanofilm. Utilizing larger submicron particles as precursors
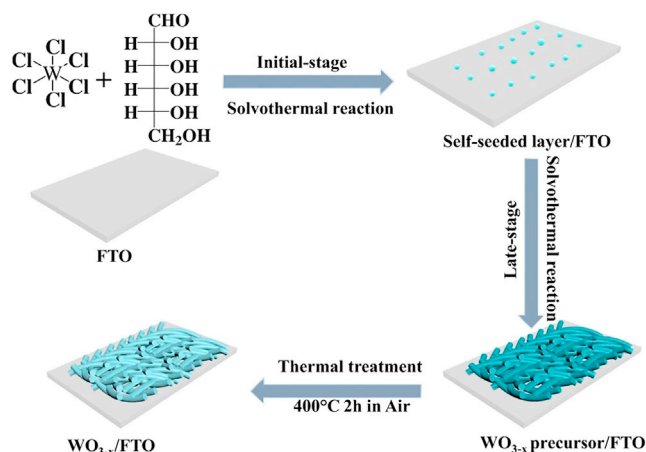
Figure 11. Schematic illustration of the synthesis of the 3D WO_{3-x} NWNs/FTO electrode

Copyright © 2023 Springer Nature Limited. Reprinted with permission from ref.[193] Copyright© 2023 Springer Nature Limited.

for nanomaterial synthesis can alleviate material costs and operational complexities. By optimizing thin film deposition parameters, the cyclic durability of WO_x thin films under repeated voltage can be markedly enhanced. The overarching goal is to refine the efficiency and quality of WO_x material preparation methods while preserving its intrinsic performance.

(2) The use of precious metal doping to enhance EC efficiency can result in significant economic and environmental resource costs. Improper handling of certain metals can lead to environmental pollution and indirectly increase the cost of subsequent material processing. Consequently, it is crucial to explore WO_x composite materials that offer high EC efficiency at a low cost. TiO_2 has shown potential in improving the optical properties of WO_x-based materials; however, it has limitation such as poor fatigue resistance and inability to withstand bending. Therefore, finding a balance between organic EC devices and inorganic composite materials can be benefited as they can compensate for each other's weaknesses. This approach holds promise as a novel research direction in the field of electrochromism, offering opportunities for the development of more efficient and versatile EC materials while considering environmental sustainability.

(3) The research and development of WO_x as EC material should prioritize improving the lifespan and response switching time of EC film, as these factors are closely related to their application. One approach to enhance performance is synthesis of WOx with specific functional groups. For example, researchers have proposed a method where WO_x reacts with the hydroxyl group on the surface of ITO to improve the adhesion and EC properties of the film on the substrate. However, ITO has limitations in terms of repeated bending and the scarcity of indium, which restricts its wider use. Therefore, reducing the cost of ITO and exploring alternative materials that are more adaptable will be important areas for future research efforts.

(4) At present, single-phase EC film materials have noticeable defects which can manifest as single or multiple deficiencies. Exploring the unique composite properties of nanocomposites represents a promising research direction for improving EC properties. The interfacial property of nanomaterials plays a crucial role in influencing electrochromism. For instance, the development of nanocrystalline WO_x film, mesoporous WO_x film, and layered WO_x hollow shell has demonstrated significant improvement in EC properties. However, further clarification is required to understand the determination of nanomaterial interfaciality. Specifically, in order to control the electron mobility of nano-WO_x, it is important to identify and maintain the appropriate form of the materials, especially the material with interfacial covalent bonds. By deepening our understanding of the reasons behind the enhanced EC effects observed in various forms of nano-WO_x, we can identify the directions for future efforts aimed at achieving superior EC devices.

(5) In terms of alleviating environmental pollution and meeting global energy demand, WO_x has a relatively low conduction band level higher than the reduction potential of O_2/O_2, leading to limited reduction of O_2 molecules during photocatalytic degradation. Various approaches, such as metal and non-metal doping, heterojunctions, and band-gap engineering, have been explored to address this issue. In catalytic reactions, the recombination of electron-hole pairs can hinder the efficiency of the process. To overcome this, heteroatoms are introduced to adjust the band structure of graphene and reduce the recombination rate of electron-hole pairs. However, further investigation and research are required to better understand the structural characteristics and functions of doped WO_x.

(6) WO_x-based nanocomposites have photocatalytic properties and can degrade and regenerate heavy metals and organic pollutants such as dyes and antibiotics in wastewater. Most of the new WO_x-based nanocomposites found in recent studies generally have outstanding photocatalytic degradation effects only for some pollutants. Most of the experiments of WO_x-based nano-photocatalysts only stay in the laboratory simulation test stage, and cannot clarify the degradation of pollutants in actual water samples. Moreover, the price of WO_x is relatively expensive, and the inexpensive photocatalyst is the main demand for the practical application of degrading pollutants, which also makes WO_x-based nano-photocatalysts still have a way to go to market applications.

AUTHOR CONTRIBUTIONS

S.Z. and Z.Y. wrote the original draft in the synthesis part. X.F. and J.Z.wrote the original draft in the application-related part. K.T. conducted a response review and revised the review manuscript. N.W. and Y.Z. supervised the study. All authors have reviewed and given approval to the final version of the manuscript.

DECLARATION OF INTERESTS

The authors declare no competing interests.

REFERENCES

1. Alturki, A. (2022). The Global Carbon Footprint and How New Carbon Mineralization Technologies Can Be Used to Reduce CO2 Emissions. ChemEngineering 6, 44. https://doi.org/10.3390/chemengineering6030044.

2. Huang, L., Krigsvoll, G., Johansen, F., Liu, Y., and Zhang, X. (2018). Carbon emission of global construction sector. Renew. Sustain. Energy Rev. 81, 1906–1916. https://doi.org/10.1016/j.rser.2017.06.001.

3. Granqvist, C.G., Arvizu, M.A., Bayrak Pehlivan, İ., Qu, H.Y., Wen, R.T., and Niklasson, G.A. (2018). Electrochromic materials and devices for energy efficiency and human comfort in buildings: A critical review. Electrochim. Acta 259, 1170–1182. https://doi.org/10.1016/j.electacta.2017.11.169.

4. Ke, Y., Chen, J., Lin, G., Wang, S., Zhou, Y., Yin, J., Lee, P.S., and Long, Y. (2019). Smart Windows: Electro-Thermo-Mechano-Photochromics, and Beyond. Adv. Energy Mater. 9, 1902066. https://doi.org/10.1002/aenm.201902066.

5. Nundy, S., Mesloub, A., Alsolami, B.M., and Ghosh, A. (2021). Electrically actuated visible and near-infrared regulating switchable smart window for energy positive building: A review. J. Clean. Prod. 301, 126854. https://doi.org/10.1016/j.jclepro.2021.126854.

6. Tan, M.-Y., Chan, K.-Y., Eldjilali, C.Z., Abdelhamed, A.H.E., Soon How Thien, G., Au, B.W.C., Goh, B.T., and Murthy, H.C.A. (2023). Rapid post-annealing effect on the TiO2-based electrochromic films. Opt. Mater. 145, 114455. https://doi.org/10.1016/j.optmat.2023.114455.

7. Rosseinsky, D.R., and Mortimer, R.J. (2001). Electrochromic Systems and the Prospects for Devices. Adv. Mater. 13, 783–793. https://doi.org/10.1002/1521-4095(200106)13:11<783::AID-ADMA783>3.0.CO;2-D.

8. Korgel, B.A. (2013). Composite for smarter windows. Nature 500, 278–279. https://doi.org/10.1038/500278a.

9. Österholm, A.M., Shen, D.E., Kerszulis, J.A., Bulloch, R.H., Kuepfert, M., Dyer, A.L., and Reynolds, J.R. (2015). Four shades of brown: tuning of electrochromic polymer blends toward high-contrast eyewear. ACS Appl. Mater. Interfaces 7, 1413–1421. https://doi.org/10.1021/am507063d.

10. Farahmand Nejad, M.A., Ranjbar, S., Parolo, C., Nguyen, E.P., Álvarez-Diduk, R., Merkoçi, A., Reza, M., and Merkoçi, A. (2021). Electrochromism: An emerging and promising approach in (bio)sensing technology. Mater. Today 50, 476–498. https://doi.org/10.1016/j.mattod.2021.06.015.

11. Zhan, Y., Yang, Z., Xu, Z., Hu, Z., Bai, X., Ren, Y., Li, M., Ullah, A., Khan, I., Qiu, J., et al. (2020). Electrochromism induced reversible upconversion luminescence modulation of WO3:Yb3+, Er3+ inverse opals for optical storage application. Chem. Eng. J. 394, 124967. https://doi.org/10.1016/j.cej.2020.124967.

12. Zhang, S., Cao, S., Zhang, T., Fisher, A., and Lee, J.Y. (2018). Al3+ intercalation/de-intercalation-enabled dual-band electrochromic smart windows with a high optical modulation, quick response and long cycle life. Energy Environ. Sci. 11, 2884–2892. https://doi.org/10.1039/c8ee01718b.

13. Yun, T.G., Park, M., Kim, D.H., Kim, D., Cheong, J.Y., Bae, J.G., Han, S.M., and Kim, I.D. (2019). All-Transparent Stretchable Electrochromic Supercapacitor Wearable Patch Device. ACS Nano 13, 3141–3150. https://doi.org/10.1021/acsnano.8b08560.

14. Wang, Y., Jiang, H., Zheng, R., Pan, J., Niu, J., Zou, X., and Jia, C. (2020). A flexible, electrochromic, rechargeable Zn-ion battery based on actiniae-like self-doped polyaniline cathode. J. Mater. Chem. A Mater. 8, 12799–12809. https://doi.org/10.1039/d0ta04203j.

15. Wang, J., Wang, X., Cong, S., Geng, F., and Zhao, Z. (2020). Fusing electrochromic technology with other advanced technologies: A new roadmap for future development. Mater. Sci. Eng. R Rep. 140, 100524. https://doi.org/10.1016/j.mser.2019.100524.

16. Kim, H.N., Cho, S.M., Ah, C.S., Song, J., Ryu, H., Kim, Y.H., and Kim, T.-Y. (2016). Electrochromic mirror using viologen-anchored nanoparticles. Mater. Res. Bull. 82, 16–21. https://doi.org/10.1016/j.materresbull.2016.03.010.

17. Tong, Z., Liu, S., Li, X., Zhao, J., and Li, Y. (2018). Self-supported one-dimensional materials for enhanced electrochromism. Nanoscale Horiz. 3, 261–292. https://doi.org/10.1039/c8nh00016f.

18. Lahav, M., and van der Boom, M.E. (2018). Polypyridyl Metallo-Organic Assemblies for Electrochromic Applications. Adv. Mater. 30, 1706641. https://doi.org/10.1002/adma.201706641.

19. Monica, S.E.S., Dhas, C.R., Venkatesh, R., Sivakumar, R., Vignesh, R., and Ferby, V.A. (2022). Nebulizer sprayed nickel-manganese (Ni-Mn) mixed metal oxide nanocomposite coatings for high-performance electrochromic device applications. J. Solid State Electrochem. 26, 1271–1290. https://doi.org/10.1007/s10008-022-05159-1.

20. Thakur, V.K., Ding, G., Ma, J., Lee, P.S., and Lu, X. (2012). Hybrid Materials and Polymer Electrolytes for Electrochromic Device Applications. Adv. Mater. 24, 4071–4096. https://doi.org/10.1002/adma.201200213.

21. Preface by the Co-Editors (2007). Annual Review of Materials Research. Annu. Rev. Mater. Res. 37. https://doi.org/10.1146/annurev.mr.37.071707.100001.

22. Sarkar, M., Dutta, T.K., and Patra, A. (2021). Two dimensional Covalent Organic Frameworks for Electrochromic Switching. Chem. Asian J. 16, 3055–3067. https://doi.org/10.1002/asia.202100815.

23. Au, B.W.C., and Chan, K.Y. (2022). Towards an All-Solid-State Electrochromic Device: A Review of Solid-State Electrolytes and the Way Forward. Polymers 14, 2458. https://doi.org/10.3390/polym14122458.

24. Runnerstrom, E.L., Llordés, A., Lounis, S.D., and Milliron, D.J. (2014). Nanostructured electrochromic smart windows: traditional materials and NIR-selective plasmonic nanocrystals. Chem. Commun. 50, 10555–10572. https://doi.org/10.1039/c4cc03109a.

25. Wu, W., Wang, M., Ma, J., Cao, Y., and Deng, Y. (2018). Electrochromic Metal Oxides: Recent Progress and Prospect. Adv. Electron. Mater. 4, 1800185. https://doi.org/10.1002/aelm.201800185.

26. Yang, P., Sun, P., and Mai, W. (2016). Electrochromic energy storage devices. Mater. Today 19, 394–402. https://doi.org/10.1016/j.mattod.2015.11.007.

27. Granqvist, C.G. (2014). Electrochromics for smart windows: Oxide-based thin films and devices. Thin Solid Films 564, 1–38. https://doi.org/10.1016/j.tsf.2014.02.002.

28. Hacioglu, S.O. (2019). Copolymerization of Azobenzene-bearing Monomer and 3,4-Ethylenedioxythiophene (EDOT): Improved Electrochemical Performance for Electrochromic Device Applications. Chin. J. Polym. Sci. 38, 109–117. https://doi.org/10.1007/s10118-019-2306-0.

29. Kim, J., Ong, G.K., Wang, Y., LeBlanc, G., Williams, T.E., Mattox, T.M., Helms, B.A., and Milliron, D.J. (2015). Nanocomposite Architecture for Rapid, Spectrally-Selective Electrochromic Modulation of Solar Transmittance. Nano Lett. 15, 5574–5579. https://doi.org/10.1021/acs.nanolett.5b02197.

30. Cong, S., Tian, Y., Li, Q., Zhao, Z., and Geng, F. (2014). Single-crystalline tungsten oxide quantum dots for fast pseudocapacitor and electrochromic applications. Adv. Mater. 26, 4260–4267. https://doi.org/10.1002/adma.201400447.

31. Liu, L., Layani, M., Yellinek, S., Kamyshny, A., Ling, H., Lee, P.S., Magdassi, S., and Mandler, D. (2014). "Nano to nano" electrodeposition of WO3 crystalline nanoparticles for electrochromic coatings. J. Mater. Chem. A 2, 16224–16229. https://doi.org/10.1039/c4ta03431g.

32. Cai, G., Tu, J., Zhou, D., Li, L., Zhang, J., Wang, X., and Gu, C. (2014). Constructed TiO2/NiO Core/Shell Nanorod Array for Efficient Electrochromic Application. J. Phys. Chem. C 118, 6690–6696. https://doi.org/10.1021/jp500699u.

33. Zhang, J.H., Cai, G.F., Zhou, D., Tang, H., Wang, X.L., Gu, C.D., and Tu, J.P. (2014). Co-doped NiO nanoflake array films with enhanced electrochromic properties. J. Mater. Chem. C 2, 7013–7021. https://doi.org/10.1039/c4tc01033g.

34. Cai, G., Wang, J., and Lee, P.S. (2016). Next-Generation Multifunctional Electrochromic Devices. Acc. Chem. Res. 49, 1469–1476. https://doi.org/10.1021/acs.accounts.6b00183.

35. Zhao, B., Zhang, X., Dong, G., Wang, H., and Yan, H. (2015). Efficient electrochromic device based on sol–gel prepared WO3 films. Ionics 21, 2879–2887. https://doi.org/10.1007/s11581-015-1471-6.

36. Cong, S., Geng, F., and Zhao, Z. (2016). Tungsten Oxide Materials for Optoelectronic Applications. Adv. Mater. 28, 10518–10528. https://doi.org/10.1002/adma.201601109.

37. Zhang, L., Wang, H., Liu, J., Zhang, Q., and Yan, H. (2020). Nonstoichiometric tungsten oxide: structure, synthesis, and applications. J. Mater. Sci. Mater. Electron. 31, 861–873. https://doi.org/10.1007/s10854-019-02596-z.

38. Zhang, M., Yang, C., Zhang, Z., Tian, W., Hui, B., Zhang, J., and Zhang, K. (2022). Tungsten oxide polymorphs and their multifunctional applications. Adv. Colloid Interface Sci. 300, 102596. https://doi.org/10.1016/j.cis.2021.102596.

39. Pan, J., Wang, Y., Zheng, R., Wang, M., Wan, Z., Jia, C., Weng, X., Xie, J., and Deng, L. (2019). Directly grown high-performance WO3 films by a novel one-step hydrothermal method with significantly improved stability for electrochromic applications. J. Mater. Chem. A 7, 13956–13967. https://doi.org/10.1039/c9ta01333d.

40. Rao, T., Zhou, Y., Jiang, J., Yang, P., and Liao, W. (2022). Low dimensional transition metal oxide towards advanced electrochromic devices. Nano Energy 100, 107479. https://doi.org/10.1016/j.nanoen.2022.107479.

41. Niklasson, G.A., and Granqvist, C.G. (2007). Electrochromics for smart windows: thin films of tungsten oxide and nickel oxide, and devices based on these. J. Mater. Chem. 17, 127–156. https://doi.org/10.1039/B612174H.

42. Ozkan, E., and Edwin, S.-H.L.C. (2002). Comparison of electrochromic amorphous and crystalline tungsten oxide films. Sol. Energy Mater. Sol. Cells 79, 439–448. https://doi.org/10.1016/S0927-0248(03)00019-9.

43. Hidayat, D., Purwanto, A., Wang, W.-N., and Okuyama, K. (2010). Preparation of size-controlled tungsten oxide nanoparticles and evaluation of their adsorption performance. Mater. Res. Bull. 45, 165–173.

44. Zhao, Y.M., Li, Y.H., Ahmad, I., McCartney, D.G., Zhu, Y.Q., and Hu, W.B. (2006). Two-dimensional tungsten oxide nanowire

networks. Appl. Phys. Lett. *89*. https://doi.org/10.1063/1.2357609.

45. Pirker, L., and Višić, B. (2022). Recent Progress in the Synthesis and Potential Applications of Two-Dimensional Tungsten (Sub)oxides. Isr. J. Chem. *62*, e202100074. https://doi.org/10.1002/ijch.202100074.

46. Surnev, S., and Netzer, F.P. (2022). Tungsten and molybdenum oxide nanostructures: two-dimensional layers and nanoclusters. J. Phys. Condens. Matter *34*, 233001. https://doi.org/10.1088/1361-648X/ac4ceb.

47. Magnéli, A., Andersson, G., Sundkvist, G., and Sundkvist, G. (1955). On the MoO2 Structure Type. Acta Chem. Scand. *9*, 1378–1381. https://doi.org/10.3891/acta.chem.scand.09-1378.

48. Gerand, B., Nowogrocki, G., Guenot, J., and Figlarz, M. (1979). Structural study of a new hexagonal form of tungsten trioxide. J. Solid State Chem. *29*, 429–434. https://doi.org/10.1016/0022-4596(79)90199-3.

49. Granqvist, C.G. (2000). Electrochromic tungsten oxide films: Review of progress 1993–1998. Sol. Energy Mater. Sol. Cell. *60*, 201–262. https://doi.org/10.1016/S0927-0248(99)00088-4.

50. Kharade, R.R., Mane, S.R., Mane, R.M., Patil, P.S., and Bhosale, P.N. (2010). Synthesis and characterization of chemically grown electrochromic tungsten oxide. J. Sol. Gel Sci. Technol. *56*, 177–183. https://doi.org/10.1007/s10971-010-2291-9.

51. Marsen, B., Cole, B., and Miller, E.L. (2007). Influence of sputter oxygen partial pressure on photoelectrochemical performance of tungsten oxide films. Sol. Energy Mater. Sol. Cell. *91*, 1954–1958. https://doi.org/10.1016/j.solmat.2007.08.008.

52. Gesheva, K., Szekeres, A., and Ivanova, T. (2003). Optical properties of chemical vapor deposited thin films of molybdenum and tungsten based metal oxides. Sol. Energy Mater. Sol. Cell. *76*, 563–576. https://doi.org/10.1016/S0927-0248(02)00267-2.

53. Bamwenda, G.R., Sayama, K., and Arakawa, H. (1999). The effect of selected reaction parameters on the photoproduction of oxygen and hydrogen from a WO3–Fe2+–Fe3+ aqueous suspension. J. Photochem. Photobiol. Chem. *122*, 175–183. https://doi.org/10.1016/S1010-6030(99)00026-X.

54. González-Borrero, P.P., Sato, F., Medina, A.N., Baesso, M.L., Bento, A.C., Baldissera, G., Persson, C., Niklasson, G.A., Granqvist, C.G., and Ferreira da Silva, A. (2010). Optical band-gap determination of nanostructured WO3 film. Appl. Phys. Lett. *96*. https://doi.org/10.1063/1.3313945.

55. Tosoni, S., Di Valentin, C., and Pacchioni, G. (2014). Effect of Alkali Metals Interstitial Doping on Structural and Electronic Properties of WO3. J. Phys. Chem. C *118*, 3000–3006. https://doi.org/10.1021/jp4123387.

56. Wang, F., Di Valentin, C., and Pacchioni, G. (2011). Electronic and Structural Properties of WO3: A Systematic Hybrid DFT Study. J. Phys. Chem. C *115*, 8345–8353. https://doi.org/10.1021/jp201057m.

57. Miller, E.L., Marsen, B., Cole, B., and Lum, M. (2006). Low-Temperature Reactively Sputtered Tungsten Oxide Films for Solar-Powered Water Splitting Applications. Electrochem. Solid State Lett. *9*, G248. https://doi.org/10.1149/1.2201994.

58. Lee, S.-H., Deshpande, R., Parilla, P., Jones, K., To, B., Mahan, A., and Dillon, A. (2006). Crystalline WO3 Nanoparticles for Highly Improved Electrochromic Applications.

Adv. Mater. *18*, 763–766. https://doi.org/10.1002/adma.200501953.

59. Han, W., Shi, Q., and Hu, R. (2021). Advances in Electrochemical Energy Devices Constructed with Tungsten Oxide-Based Nanomaterials. Nanomaterials *11*, 692. https://doi.org/10.3390/nano11030692.

60. Thummavichai, K., Trimby, L., Wang, N., Wright, C.D., Xia, Y., and Zhu, Y. (2017). Low Temperature Annealing Improves the Electrochromic and Degradation Behavior of Tungsten Oxide (WOx) Thin Films. J. Phys. Chem. C *121*, 20498–20506. https://doi.org/10.1021/acs.jpcc.7b06300.

61. Parashar, M., and Ranbir, V.K.S. (2020). Metal oxides nanoparticles via sol–gel method: a review on synthesis, characterization and applications. J. Mater. Sci. Mater. Electron. *31*, 3729–3749. https://doi.org/10.1007/s10854-020-02994-8.

62. Corriu, R.J.P., and Leclercq, D. (1996). Recent Developments of Molecular Chemistry for Sol–Gel Processes. Angew. Chem. Int. Ed. Engl. *35*, 1420–1436. https://doi.org/10.1002/anie.199614201.

63. Au, B.W.-C., and Chan, K.-Y. (2020). Effect of precursor solution stirring time on the electrochromic performance of tungsten oxide films. Surf. Eng. *36*, 94–99. https://doi.org/10.1080/02670844.2019.1622264.

64. Jittiarporn, P., and Simona, B.M.N. (2017). Electrochromic properties of solegel prepared hybrid transition metal oxides - A short review. J. Sci. Adv. Mater. Devices *2*, 286–300. https://doi.org/10.1016/j.jsamd.2017.08.005.

65. Chai, Y., Ha, F.Y., Yam, F.K., and Hassan, Z. (2016). Fabrication of Tungsten Oxide Nanostructure by Sol-Gel Method. Procedia Chem. *19*, 113–118. https://doi.org/10.1016/j.proche.2016.03.123.

66. Au, B.W.-C., Yeoh, M.E., Sahdan, M.Z., Murthy, H.C.A., Chan, K.Y., and Thien, G.S.H. (2023). The Effect of Transparent Conducting Oxide Films on WO3-Based Electrochromic Devices with Conducting Polymer Electrolytes. Polymers *15*, 238. https://doi.org/10.3390/nano11030692.

67. Jiang, Y., Chen, Y., Liu, Y.-J., and Sui, G.-X. (2018). Lightweight spongy bone-like graphene@SiC aerogel composites for high-performance microwave absorption. Chem. Eng. J. *337*, 522–531. https://doi.org/10.1016/j.cej.2017.12.131.

68. Gao, X., Yang, C., Xiao, F., Zhu, Y., Wang, J., and Su, X. (2012). WO3·0.33H2O nanoplates: Hydrothermal synthesis, photocatalytic and gas-sensing properties. Mater. Lett. *84*, 151–153. https://doi.org/10.1016/j.matlet.2012.06.078.

69. Mohan, V.V., Anjana, P.M., and Rakhi, R.B. (2022). One pot synthesis of tungsten oxide nanomaterial and application in the field of flexible symmetric supercapacitor energy storage device. Mater. Today: Proc. *62*, 848–851. https://doi.org/10.1016/j.matpr.2022.04.046.

70. Mushtaq, K., Chou, P.M., and Lai, C.W. (2021). Review on the Synthesis Methods of Nano-Tungsten Oxide Dihydrate Colloid. MATEC Web Conf. *335*, 03008. https://doi.org/10.1051/matecconf/202133503008.

71. Thummavichai, K., Nguyen, T.H.Q., Longo, G., Qiang, D., Zoppi, G., Schlettwein, D., Maiello, P., Fleck, N., Wang, N., and Zhu, Y. (2023). Effect of metal dopants on the electrochromic performance of hydrothermally-prepared tungsten oxide

materials. RSC Adv. *13*, 35457–35467. https://doi.org/10.1039/d3ra06018g.

72. Choi, H.G., Jung, Y.H., and Kim, D.K. (2005). Solvothermal Synthesis of Tungsten Oxide Nanorod/Nanowire/Nanosheet. J. Am. Ceram. Soc. *88*, 1684–1686. https://doi.org/10.1111/j.1551-2916.2005.00341.x.

73. Sadakane, M., Sasaki, K., Kunioku, H., Ohtani, B., Ueda, W., and Abe, R. (2008). Preparation of nano-structured crystalline tungsten(VI) oxide and enhanced photocatalytic activity for decomposition of organic compounds under visible light irradiation. Chem. Commun. 6552–6554. https://doi.org/10.1039/b815214d.

74. Xie, Y., Kocaefe, D., Chen, C., and Kocaefe, Y. (2016). Review of Research on Template Methods in Preparation of Nanomaterials. J. Nanomater. *2016*, 1–10. https://doi.org/10.1155/2016/2302595.

75. Kawamura, G., Muto, H., and Matsuda, A. (2014). Hard template synthesis of metal nanowires. Front. Chem. *2*, 104. https://doi.org/10.3389/fchem.2014.00104.

76. Nielsch, K., Choi, J., Schwirn, K., Wehrspohn, R.B., and Gösele, U. (2002). Self-ordering Regimes of Porous Alumina: The 10 Porosity Rule. Nano Lett. *2*, 677–680. https://doi.org/10.1021/nl025537k.

77. Pan, J., Sun, X., Jin, Z., Zhao, Q., Qu, H., and He, J. (2022). Constructing two-dimensional lamellar monometallic carbon nanocomposites by sodium chloride hard template for lightweight microwave scattering and absorption. Compos. B Eng. *228*, 109422. https://doi.org/10.1016/j.compositesb.2021.109422.

78. Yang, Y., Yan, Y., Ren, B., Fan, C., Liu, Y., Deng, Q., Zhong, L., You, C., Xu, Y., and Yang, R. (2021). Modified nano-CaCO3 hard template method for hierarchical porous carbon powder with enhanced electrochemical performance in lithium-sulfur battery. Adv. Powder Technol. *32*, 3574–3584. https://doi.org/10.1016/j.apt.2021.08.007.

79. Weidner, E., Bartczak, P., Goscianska, J., Jesionowski, T., Jaroniec, M., and Ciesielczyk, F. (2023). Soft-templating synthesis of mesoporous alumina enriched with lanthana and its potential as diclofenac delivery system. Microporous Mesoporous Mater. *351*, 112487. https://doi.org/10.1016/j.micromeso.2023.112487.

80. Wang, H., Jin, T., Zheng, X., Jiang, B., Zhu, C., Yuan, X., Zheng, J., and Wu, M. (2016). Influence of two different template removal methods on the micromorphology, crystal structure, and photocatalytic activity of hollow CdS nanospheres. J. Nanopart. Res. *18*, 339. https://doi.org/10.1007/s11051-015-3255-3.

81. Yang, B., Barnes, P.R.F., Bertram, W., and Luca, V. (2007). Strong photoresponse of nanostructured tungsten trioxide films prepared via a sol–gel route. J. Mater. Chem. *17*, 2722–2729. https://doi.org/10.1039/B702097J.

82. Yan, B., Xu, Y., Goh, N.K., and Chia, L.S. (2000). Hydrothermal synthesis and crystal structures of two novel hybrid open-frameworks and a two-dimensional network based on tungsten(vi) oxides. Chem. Commun. 2169–2170. https://doi.org/10.1039/B005303L.

83. Atak, G., Pehlivan, B., İlknur, M., José, G., Claes, G., and Niklasson, G.A. (2021). Electrochromic tungsten oxide films prepared by sputtering: Optimizing cycling

durability by judicious choice of deposition parameters. Electrochim. Acta *367*. https://doi.org/10.1016/j.electacta.2020.137233.

84. Brigouleix, C., Topart, P., Bruneton, E., Sabary, F., Nouhaut, G., and Campet, G. (2001). Roll-to-roll pulsed dc magnetron sputtering deposition of WO3 for electrochromic windows. Electrochim. Acta *46*, 1931–1936. https://doi.org/10.1016/S0013-4686(01)00362-0.

85. Widjaja, E.J., Delporte, G., Vandevelde, F., and Vanterwyngen, B. (2008). Progress toward roll-to-roll processing of inorganic monolithic electrochromic devices on polymeric substrates. Sol. Energy Mater. Sol. Cell. *92*, 97–100. https://doi.org/10.1016/j.solmat.2007.03.030.

86. Granqvist, C.G., Bayrak Pehlivan, İ., and Niklasson, G.A. (2018). Electrochromics on a roll: Web-coating and lamination for smart windows. Surf. Coating. Technol. *336*, 133–138. https://doi.org/10.1016/j.surfcoat.2017.08.006.

87. Arvizu, M.A., Qu, H.-Y., Cindemir, U., Qiu, Z., Rojas-González, E.A., Primetzhofer, D., Granqvist, C.G., Österlund, L., and Niklasson, G.A. (2019). Electrochromic WO3 thin films attain unprecedented durability by potentiostatic pretreatment. J. Mater. Chem. A Mater. *7*, 2908–2918. https://doi.org/10.1039/C8TA09621J.

88. Deshpande, R., Lee, S.H., Mahan, A.H., Parilla, P.A., Jones, K.M., Norman, A.G., To, B., Blackburn, J.L., Mitra, S., and Dillon, A.C. (2007). Optimization of crystalline tungsten oxide nanoparticles for improved electrochromic applications. Solid State Ionics *178*, 895–900. https://doi.org/10.1016/j.ssi.2007.03.010.

89. Mahan, A.H., Parilla, P.A., Jones, K.M., and Dillon, A.C. (2005). Hot-wire chemical vapor deposition of crystalline tungsten oxide nanoparticles at high density. Chem. Phys. Lett. *413*, 88–94. https://doi.org/10.1016/j.cplett.2005.07.037.

90. Park, S., Park, H.S., Dao, T.T., Song, S.H., Lee, S., Tran, H.V., Ullah, A., Han, C.-H., and Hong, S. (2022). Solvothermal synthesis of oxygen deficient tungsten oxide nano-particle for dual band electrochromic devices. Sol. Energy Mater. Sol. Cell. *242*, 111759. https://doi.org/10.1016/j.solmat.2022.111759.

91. Santato, C., Ulmann, M., and Augustynski, J. (2001). Enhanced Visible Light Conversion Efficiency Using Nanocrystalline WO3 Films. Adv. Mater. *13*, 511–514. https://doi.org/10.1002/1521-4095(200104)13:7<511::Aid-adma511>3.0.Co;2-w.

92. Baeck, S.H., Choi, K.S., Jaramillo, T.F., Stucky, G.D., and McFarland, E.W. (2003). Enhancement of Photocatalytic and Electrochromic Properties of Electrochemically Fabricated Mesoporous WO3 Thin Films. Adv. Mater. *15*, 1269–1273. https://doi.org/10.1002/adma.200304669.

93. Chen, D., and Ye, J. (2008). Hierarchical WO3 Hollow Shells: Dendrite, Sphere, Dumbbell, and Their Photocatalytic Properties. Adv. Funct. Mater. *18*, 1922–1928. https://doi.org/10.1002/adfm.200701468.

94. Kim, K., Choi, D., Kim, H., Lee, M., Chu, W., Ahn, S.H., Chun, D.M., and Lee, C.S. (2018). Investigation of Varying Particle Sizes of Dry-Deposited WO3 Particles in Relation to Performance of Electrochromic Cell. Int. J. of Precis. Eng. and Manuf. -Green. Tech. *5*, 409–414. https://doi.org/10.1007/s40684-018-0043-4.

95. Lin, S.H., Chen, F.R., and Kai, J.J. (2008). Electrochromic properties of nano-structured nickel oxide thin film prepared by spray pyrolysis method. Appl. Surf. Sci. *254*, 2017–2022. https://doi.org/10.1016/j.apsusc.2007.08.029.

96. Jiao, Z., Wang, J., Ke, L., Liu, X., Demir, H.V., Yang, M.F., and Sun, X.W. (2012). Electrochromic properties of nanostructured tungsten trioxide (hydrate) films and their applications in a complementary electrochromic device. Electrochim. Acta *63*, 153–160. https://doi.org/10.1016/j.electacta.2011.12.069.

97. Wen-Cheun Au, B., Chan, K.Y., Tamang, A., and Knipp, D. (2020). Post-annealing effect on the electrochromic properties of WO3 films. Opt. Mater. *108*, 110426. https://doi.org/10.1016/j.optmat.2020.110426.

98. Song, Y., Zhang, Z., Yan, L., Zhang, L., Liu, S., Xie, S., Xu, L., and Du, J. (2019). Electrodeposition of Ti-Doped Hierarchically Mesoporous Silica Microspheres/Tungsten Oxide Nanocrystallines Hybrid Films and Their Electrochromic Performance. Nanomaterials *9*, 1795. https://doi.org/10.3390/nano9121795.

99. Akemann, W., Otto, A., and Schober, H.R. (1997). Raman scattering by bulk phonons in microcrystalline silver and copper via electronic surface excitations. Phys. Rev. Lett. *79*, 5050–5053. https://doi.org/10.1103/PhysRevLett.79.5050.

100. Abidi, D., Jusserand, B., and Fave, J.L. (2010). Raman scattering studies of heavily doped microcrystalline porous silicon and porous silicon free-standing membranes. Phys. Rev. B *82*, 075210. https://doi.org/10.1103/PhysRevB.82.075210.

101. Yang, K.-J., Sung, S.-J., Choi, B.-D., and Kang, J.-K. (2009). Light Scattering Characteristics of Newly Designed Polymer Dispersed Liquid Crystals Films. Mol. Cryst. Liq. Cryst. *513*, 38–44. https://doi.org/10.1080/15421400903192731.

102. Caspar, J., Dünges, B., Kirste, R.G., Heitz, T., and Wiedenmann, A. (1997). The structure of high-performance polymer blends by small-angle neutron scattering. Physica B *234–236*, 240–241. https://doi.org/10.1016/s0921-4526(96)00924-6.

103. Inomata, K., Sasaki, Y., and Nose, T. (2002). Packing manner of graft copolymers with rigid-rod main chains and amorphous-crystalline diblock copolymers as side chains. J. Polym. Sci. B Polym. Phys. *40*, 1904–1912. https://doi.org/10.1002/polb.10256.

104. Wang, H., Barrett, M., Duane, B., Gu, J., and Zenhausern, F. (2018). Materials and processing of polymer-based electrochromic devices. Mater. Sci. Eng., B *228*, 167–174. https://doi.org/10.1016/j.mseb.2017.11.016.

105. Zhang, S., Cao, S., Zhang, T., Yao, Q., Lin, H., Fisher, A., and Lee, J.Y. (2019). Overcoming the Technical Challenges in Al Anode–Based Electrochromic Energy Storage Windows. Small Methods *4*. https://doi.org/10.1002/smtd.201900545.

106. Li, H., Zhang, W., and Elezzabi, A.Y. (2020). Transparent Zinc-Mesh Electrodes for Solar-Charging Electrochromic Windows. Adv. Mater. *32*, e2003574. https://doi.org/10.1002/adma.202003574.

107. Shin, J.H., Park, J.Y., Han, S.H., Lee, Y.H., Sun, J.Y., and Choi, S.S. (2022). Color-Tuning Mechanism of Electrically Stretchable Photonic Organogels. Adv. Sci. *9*, 2202897. https://doi.org/10.1002/advs.202202897.

108. Camurlu, P. (2014). Polypyrrole derivatives for electrochromic applications. RSC Adv. *4*, 55832–55845. https://doi.org/10.1039/c4ra11827h.

109. Shin, H., Seo, S., Park, C., Na, J., Han, M., and Kim, E. (2016). Energy saving electrochromic windows from bistable low-HOMO level conjugated polymers. Energy Environ. Sci. *9*, 117–122. https://doi.org/10.1039/c5ee03160e.

110. Li, X., Perera, K., He, J., Gumyusenge, A., and Mei, J. (2019). Solution-processable electrochromic materials and devices: roadblocks and strategies towards large-scale applications. J. Mater. Chem. C Mater. *7*, 12761–12789. https://doi.org/10.1039/c9tc02861g.

111. Hassab, S., Shen, D.E., Österholm, A.M., Da Rocha, M., Song, G., Alesanco, Y., Viñuales, A., Rougier, A., Reynolds, J.R., Padilla, J., and Padilla, J. (2018). A new standard method to calculate electrochromic switching time. Sol. Energy Mater. Sol. Cell. *185*, 54–60. https://doi.org/10.1016/j.solmat.2018.04.031.

112. Bera, M.K., Mori, T., Yoshida, T., Ariga, K., and Higuchi, M. (2019). Construction of Coordination Nanosheets Based on Tris(2,2'-bipyridine)-Iron-(Fe2+) Complexes as Potential Electrochromic Materials. ACS Appl. Mater. Interfaces *11*, 11893–11903. https://doi.org/10.1021/acsami.8b22568.

113. Lim, J.W., Yoo, S.J., Park, S.H., Yun, S.U., and Sung, Y.-E. (2009). High electrochromic performance of co-sputtered vanadium–titanium oxide as a counter electrode. Sol. Energy Mater. Sol. Cell. *93*, 2069–2074. https://doi.org/10.1016/j.solmat.2009.03.008.

114. Yuan, Y.F., Xia, X.H., Wu, J.B., Gui, J.S., Chen, Y.B., and Guo, S.Y. (2010). Electrochromism in mesoporous nanowall cobalt oxide thin films prepared via lyotropic liquid crystal media with electrodeposition. J. Membr. Sci. *364*, 298–303. https://doi.org/10.1016/j.memsci.2010.08.025.

115. Pathak, D.K., Chaudhary, A., Tanwar, M., Goutam, U.K., Mondal, P., and Kumar, R. (2021). Nickel Cobalt Oxide Nanoneedles for Electrochromic Glucose Sensors. ACS Appl. Nano Mater. *4*, 2143–2152. https://doi.org/10.1021/acsanm.0c03451.

116. Jeong, C.Y., Abe, Y., Kawamura, M., Kim, K.H., and Kiba, T. (2019). Electrochromic properties of rhodium oxide thin films prepared by reactive sputtering under an O2 or H2O vapor atmosphere. Sol. Energy Mater. Sol. Cell. *200*, 109976. https://doi.org/10.1016/j.solmat.2019.109976.

117. Mortimer, R.J., and Varley, T.S. (2011). Synthesis, characterisation and in situ colorimetry of electrochromic Ruthenium purple thin films. Dyes Pigments *89*, 169–176. https://doi.org/10.1016/j.dyepig.2010.10.009.

118. Husmann, S., and Zarbin, A.J.G. (2015). Multifunctional carbon nanotubes/ruthenium purple thin films: preparation, characterization and study of application as sensors and electrochromic materials. Dalton Trans. *44*, 5985–5995. https://doi.org/10.1039/c4dt02784a.

119. Tang, X., Chen, J., Wang, Z., Hu, Z., Song, G., Zhang, S., Chen, Z., Wu, Q., Liu, M., Cong, S., and Zhao, Z. (2021). Vibrant Color Palettes of Electrochromic Manganese Oxide Electrodes for Colorful Zn-Ion Battery. Adv. Opt. Mater. 9. https://doi.org/10.1002/adom.202100637.

120. Yoshino, T., Kobayashi, K., Araki, S., Nakamura, K., and Kobayashi, N. (2012). Electrochromic properties of electrochemically fabricated nanostructure nickel oxide and manganese oxide films. Sol. Energy Mater. Sol. Cell. 99, 43–49. https://doi.org/10.1016/j.solmat.2011.08.024.

121. Lee, C.-T., Han, S., Zhao, Y.-X., Weng, K.W., Hung, Y.C., Hsu, T.H., and Hsieh, H.Y. (2019). Synthesis and electrochromic properties of molybdenum oxide films. Surf. Coating. Technol. 363, 426–429. https://doi.org/10.1016/j.surfcoat.2018.12.028.

122. Li, H., McRae, L., Firby, C.J., Al-Hussein, M., and Elezzabi, A.Y. (2018). Nanohybridization of molybdenum oxide with tungsten molybdenum oxide nanowires for solution-processed fully reversible switching of energy storing smart windows. Nano Energy 47, 130–139. https://doi.org/10.1016/j.nanoen.2018.02.043.

123. Lin, F., Nordlund, D., Weng, T.C., Moore, R.G., Gillaspie, D.T., Dillon, A.C., Richards, R.M., and Engtrakul, C. (2013). Hole doping in Al-containing nickel oxide materials to improve electrochromic performance. ACS Appl. Mater. Interfaces 5, 301–309. https://doi.org/10.1021/am302097b.

124. Avendaño, A., Azens, A., Niklasson, G.A., and Granqvist, C.G. (2007). Sputter deposited electrochromic films and devices based on these: Progress on nickel-oxide-based films. Mater. Sci. Eng., B 138, 112–117. https://doi.org/10.1016/j.mseb.2005.07.029.

125. Salvi, A.M., Decker, F., Varsano, F., and Speranza, G. (2001). Use of XPS for the study of cerium-vanadium (electrochromic) mixed oxides. Surf. Interface Anal. 31, 255–264. https://doi.org/10.1002/sia.986.

126. Zelazowska, E., and Rysiakiewicz-Pasek, E. (2009). Thin TiO2 films for an electrochromic system. Opt. Mater. 31, 1802–1804. https://doi.org/10.1016/j.optmat.2008.12.037.

127. Weng, K.-W., Han, S., Chen, Y.-C., and Wang, D.-Y. (2009). Characterization of tungsten–titanium oxide electrode for electrochromic applications. Appl. Surf. Sci. 255, 3848–3853. https://doi.org/10.1016/j.apsusc.2008.10.071.

128. Niwa, T., and Takai, O. (2010). Electrochemical, Optical and Electronic Properties of Iridium Tin Oxide Thin Film as Counter Electrode of Electrochromic Device. Jpn. J. Appl. Phys. 49, 105802. https://doi.org/10.1143/jjap.49.105802.

129. Bouvard, O., and Schüler, A. (2019). Color neutral nanocomposite nickel-tantalum oxide for electrochromic windows. J. Phys, Conf. Ser. 1343, 012192. https://doi.org/10.1088/1742-6596/1343/1/012192.

130. Patil, P.S., Kadam, L.D., and Lokhande, C.D. (1998). Studies on electrochromism of spray pyrolyzed cobalt oxide thin films. Sol. Energy Mater. Sol. Cell. 53, 229–234. https://doi.org/10.1016/S0927-0248(98)00006-3.

131. Kadam, L.D., Pawar, S.H., and Patil, P.S. (2001). Studies on ionic intercalation properties of cobalt oxide thin films prepared by spray pyrolysis technique.

Mater. Chem. Phys. 68, 280–282. https://doi.org/10.1016/S0254-0584(00)00365-5.

132. Ma, S.S.K., Maeda, K., Abe, R., and Domen, K. (2012). Visible-light-driven nonsacrificial water oxidation over tungsten trioxide powder modified with two different cocatalysts. Energy Environ. Sci. 5, 8390. https://doi.org/10.1039/c2ee21801a.

133. Zheng, H., Ou, J.Z., Strano, M.S., Kaner, R.B., Mitchell, A., and Kalantar-Zadeh, K. (2011). Nanostructured Tungsten Oxide - Properties, Synthesis, and Applications. Adv. Funct. Mater. 21, 2175–2196. https://doi.org/10.1002/adfm.201002477.

134. Abe, R., Takami, H., Murakami, N., and Ohtani, B. (2008). Pristine Simple Oxides as Visible Light Driven Photocatalysts: Highly Efficient Decomposition of Organic Compounds over Platinum-Loaded Tungsten Oxide. J. Am. Chem. Soc. 130, 7780–7781. https://doi.org/10.1021/ja800835q.

135. Huang, Z.F., Song, J., Pan, L., Zhang, X., Wang, L., and Zou, J.J. (2015). Tungsten Oxides for Photocatalysis, Electrochemistry, and Phototherapy. Adv. Mater. 27, 5309–5327. https://doi.org/10.1002/adma.201501217.

136. Takeda, H., and Adachi, K. (2007). Near Infrared Absorption of Tungsten Oxide Nanoparticle Dispersions. J. Am. Ceram. Soc. 90, 4059–4061. https://doi.org/10.1111/j.1551-2916.2007.02065.x.

137. Mortimer, R.J. (1999). Organic electrochromic materials. Electrochim. Acta 44, 2971–2981. https://doi.org/10.1016/S0013-4686(99)00046-8.

138. Andersson, P., Forchheimer, R., Tehrani, P., and Berggren, M. (2007). Printable All-Organic Electrochromic Active-Matrix Displays. Adv. Funct. Mater. 17, 3074–3082. https://doi.org/10.1002/adfm.200601241.

139. Zhang, W., Li, H., Yu, W.W., and Elezzabi, A.Y. (2020). Transparent inorganic multicolour displays enabled by zinc-based electrochromic devices. Light Sci. Appl. 9, 121. https://doi.org/10.1038/s41377-020-00366-9.

140. Wang, Z., Wang, X., Cong, S., Chen, J., Sun, H., Chen, Z., Song, G., Geng, F., Chen, Q., and Zhao, Z. (2020). Towards full-colour tunability of inorganic electrochromic devices using ultracompact fabry-perot nanocavities. Nat. Commun. 11, 302. https://doi.org/10.1038/s41467-019-14194-y.

141. Sydam, R., and Deepa, M. (2013). A new organo-inorganic hybrid of poly(cyclotri phosphazene-4,4′-bipyridinium)chloride with a large electrochromic contrast. J. Mater. Chem. C Mater. 1, 7930. https://doi.org/10.1039/c3tc31486c.

142. Banasz, R., and Wałęsa-Chorab, M. (2019). Polymeric complexes of transition metal ions as electrochromic materials: Synthesis and properties. Coord. Chem. Rev. 389, 1–18. https://doi.org/10.1016/j.ccr.2019.03.009.

143. Williams, R.M., Cola, L.D., Hartl, F., Lagref, J.J., Planeix, J.M., Cian, A.D., and Hosseini, M.W. (2002). Photophysical, electrochemical and electrochromic properties of copper-bis(4,4′-dimethyl-6,6′-diphenyl-2,2′-bipyridine) complexes. Coord. Chem. Rev. 230, 253–261. https://doi.org/10.1016/S0010-8545(02)00046-2.

144. Baran, D., Balan, A., Celebi, S., Meana Esteban, B., Neugebauer, H., Sariciftci, N.S., Toppare, L., and Toppare, L. (2010).

Processable Multipurpose Conjugated Polymer for Electrochromic and Photovoltaic Applications. Chem. Mater. 22, 2978–2987. https://doi.org/10.1021/cm100372t.

145. Fu, H., Yan, S., Yang, T., Yin, M., Zhang, L., Shao, X., Dong, Y., Li, W., and Zhang, C. (2022). New dual conjugated polymer electrochromic device with remarkable yellow-to-green switch for adaptive camouflage. Chem. Eng. J. 438, 135455. https://doi.org/10.1016/j.cej.2022.135455.

146. Antoni, P.W., Golz, C., and Hansmann, M.M. (2022). Organic Four-Electron Redox Systems Based on Bipyridine and Phenanthroline Carbene Architectures. Angew. Chem. Int. Ed. Engl. 61, e202203064. https://doi.org/10.1002/anie.202203064.

147. Yan, J., Wang, T., Wu, G., Dai, W., Guan, N., Li, L., and Gong, J. (2015). Tungsten oxide single crystal nanosheets for enhanced multichannel solar light harvesting. Adv. Mater. 27, 1580–1586. https://doi.org/10.1002/adma.201404792.

148. Miseki, Y., Kusama, H., Sugihara, H., and Sayama, K. (2010). Cs-Modified WO3 Photocatalyst Showing Efficient Solar Energy Conversion for O2 Production and Fe (III) Ion Reduction under Visible Light. J. Phys. Chem. Lett. 1, 1196–1200. https://doi.org/10.1021/jz100233w.

149. Wang, F., Di Valentin, C., and Pacchioni, G. (2012). Doping of WO3 for Photocatalytic Water Splitting: Hints from Density Functional Theory. J. Phys. Chem. C 116, 8901–8909. https://doi.org/10.1021/jp300867j.

150. Chen, D., Gao, L., Yasumori, A., Kuroda, K., and Sugahara, Y. (2008). Size- and shape-controlled conversion of tungstate-based inorganic-organic hybrid belts to WO3 nanoplates with high specific surface areas. Small 4, 1813–1822. https://doi.org/10.1002/smll.200800205.

151. Chen, X., Zhou, Y., Liu, Q., Li, Z., Liu, J., and Zou, Z. (2012). Ultrathin, single-crystal WO(3) nanosheets by two-dimensional oriented attachment toward enhanced photocatalytic reduction of CO(2) into hydrocarbon fuels under visible light. ACS Appl. Mater. Interfaces 4, 3372–3377. https://doi.org/10.1021/am300661s.

152. Wang, G., Ling, Y., Wang, H., Yang, X., Wang, C., Zhang, J.Z., and Li, Y. (2012). Hydrogen-treated WO3 nanoflakes show enhanced photostability. Energy Environ. Sci. 5, 6180. https://doi.org/10.1039/c2ee03158b.

153. Liu, G., Han, J., Zhou, X., Huang, L., Zhang, F., Wang, X., Ding, C., Zheng, X., Han, H., and Li, C. (2013). Enhancement of visible-light-driven O2 evolution from water oxidation on WO3 treated with hydrogen. J. Catal. 307, 148–152. https://doi.org/10.1016/j.jcat.2013.06.024.

154. Solarska, R., Królikowska, A., and Augustyński, J. (2010). Silver nanoparticle induced photocurrent enhancement at WO3 photoanodes. Angew. Chem. Int. Ed. Engl. 49, 7980–7983. https://doi.org/10.1002/anie.201002173.

155. Zhou, K., Wang, H., Liu, J., Zhao, B., Zhang, Q., and Yan, H. (2020). Ions Transport Control in Electrochromic WO3 Film for the Cyclic Stability Study. J. Electrochem. Soc. 167, 106502. https://doi.org/10.1149/1945-7111/ab98aa.

156. Cai, G.F., Tu, J.P., Zhou, D., Wang, X.L., and Gu, C.D. (2014). Growth of vertically aligned hierarchical WO3 nano-architecture arrays on transparent conducting substrates with outstanding electrochromic performance. Sol. Energy Mater. Sol. Cell. *124*, 103–110. https://doi.org/10.1016/j.solmat.2014.01.042.

157. Zhang, B., Yuan, P., Xu, G., Chen, Z., Li, Z., Ye, H., Wang, J., Shi, P., and Sun, X. (2021). DUSP6 expression is associated with osteoporosis through the regulation of osteoclast differentiation via ERK$_2$/Smad$_2$ signaling. Cell Death Dis. *12*, 825. https://doi.org/10.1038/s41419-021-04110-y.

158. Li, H., Wang, J., Shi, Q., Zhang, M., Hou, C., Shi, G., Wang, H., Zhang, Q., Li, Y., and Chi, Q. (2016). Constructing three-dimensional quasi-vertical nanosheet architectures from self-assemble two-dimensional WO 3 ·2H 2 O for efficient electrochromic devices. Appl. Surf. Sci. *380*, 281–287. https://doi.org/10.1016/j.apsusc.2016.01.009.

159. Liang, L., Zhang, J., Zhou, Y., Xie, J., Zhang, X., Guan, M., Pan, B., and Xie, Y. (2013). High-performance flexible electrochromic device based on facile semiconductor-to-metal transition realized by WO$_3$.2H$_2$O ultrathin nanosheets. Sci. Rep. *3*, 1936. https://doi.org/10.1038/srep01936.

160. Novak, T.G., Kim, J., Tiwari, A.P., Kim, J., Lee, S., Lee, J., and Jeon, S. (2020). 2D MoO$_3$ Nanosheets Synthesized by Exfoliation and Oxidation of MoS$_2$ for High Contrast and Fast Response Time Electrochromic Devices. ACS Sustain. Chem. Eng. *8*, 11276–11282. https://doi.org/10.1021/acssuschemeng.0c03191.

161. Liu, Y., Sakamoto, R., Ho, C.-L., Nishihara, H., and Wong, W.-Y. (2019). Electrochromic triphenylamine-based cobalt(ii) complex nanosheets. J. Mater. Chem. C Mater. *7*, 9159–9166. https://doi.org/10.1039/c9tc02257k.

162. Wu, W., Fang, H., Ma, H., Wu, L., Wang, Q., and Wang, H. (2021). Self-Powered Rewritable Electrochromic Display based on WO(3-x) Film with Mechanochemically Synthesized MoO$_{(3-y)}$ Nanosheets. ACS Appl. Mater. Interfaces *13*, 20326–20335. https://doi.org/10.1021/acsami.1c01959.

163. Wang, L., Yuan, L., Wu, X., Wu, J., Hou, C., and Feng, S. (2014). Electrochromic response of pulsed laser deposition prepared WO3–TiO$_2$composite film. RSC Adv. *4*, 47670–47676. https://doi.org/10.1039/c4ra07138g.

164. Xu, J., Zhang, Y., Zhai, T.T., Kuang, Z., Li, J., Wang, Y., Gao, Z., Song, Y.Y., and Xia, X.H. (2018). Electrochromic-Tuned Plasmonics for Photothermal Sterile Window. ACS Nano *12*, 6895–6903. https://doi.org/10.1021/acsnano.8b02292.

165. Gu, H., Guo, C., Zhang, S., Bi, L., Li, T., Sun, T., and Liu, S. (2018). Highly Efficient, Near-Infrared and Visible Light Modulated Electrochromic Devices Based on Polyoxometalates and W(18)O(49) Nanowires. ACS Nano *12*, 559–567. https://doi.org/10.1021/acsnano.7b07360.

166. Wang, J., Zhou, Y., Zhao, W., Niu, Y., Mao, Y., and Cheng, W. (2023). Amorphous Mixed-Vanadium-Tungsten Oxide Films as Optically Passive Ion Storage Materials for Solid-State Near-Infrared Electrochromic Devices. ACS Appl. Mater. Interfaces *15*, 7120–7128. https://doi.org/10.1021/acsami.2c20635.

167. Shi, Y., Zhang, Y., Tang, K., Cui, J., Shu, X., Wang, Y., Liu, J., Jiang, Y., Tan, H.H., and Wu, Y. (2019). Designed growth of WO3/ PEDOT core/shell hybrid nanorod arrays with modulated electrochromic properties. Chem. Eng. J. *355*, 942–951. https://doi.org/10.1016/j.cej.2018.08.163.

168. Cai, G.F., Tu, J.P., Zhou, D., Zhang, J.H., Wang, X.L., and Gu, C.D. (2014). Dual electrochromic film based on WO3/ polyaniline core/shell nanowire array. Sol. Energy Mater. Sol. Cell. *122*, 51–58. https://doi.org/10.1016/j.solmat.2013.11.015.

169. Sakamoto, R., Takada, K., Sun, X., Pal, T., Tsukamoto, T., Phua, E.J.H., Rapakousiou, A., Hoshiko, K., and Nishihara, H. (2016). The coordination nanosheet (CONASH). Coord. Chem. Rev. *320–321*, 118–128. https://doi.org/10.1016/j.ccr.2015.12.001.

170. Hou, Y., Du, X., Scheiner, S., McMeekin, D.P., Wang, Z., Li, N., Killian, M.S., Chen, H., Richter, M., Levchuk, I., et al. (2017). A generic interface to reduce the efficiency-stability-cost gap of perovskite solar cells. Science *358*, 1192–1197. https://doi.org/10.1126/science.aao5561.

171. Dinca, V., Liu, Q., Brajnicov, S., Bonciu, A., Vlad, A., and Dinu, C.Z. (2020). Composites formed from tungsten trioxide and graphene oxide for the next generation of electrochromic interfaces. Compos. Commun. *17*, 115–122. https://doi.org/10.1016/j.coco.2019.11.015.

172. Khan, A., Bhosale, N.Y., Mali, S.S., Hong, C.K., and Kadam, A.V. (2020). Reduced graphene oxide layered WO(3) thin film with enhanced electrochromic properties. J. Colloid Interface Sci. *571*, 185–193. https://doi.org/10.1016/j.jcis.2020.03.029.

173. De, S., Higgins, T.M., Lyons, P.E., Doherty, E.M., Nirmalraj, P.N., Blau, W.J., Boland, J.J., and Coleman, J.N. (2009). Silver Nanowire Networks as Flexible, Transparent, Conducting Films: Extremely High DC to Optical Conductivity Ratios. ACS Nano *3*, 1767–1774. https://doi.org/10.1021/nn900348c.

174. Li, H., Lv, Y., Zhang, X., Wang, X., and Liu, X. (2015). High-performance ITO-free electrochromic films based on bi-functional stacked WO$_3$/Ag/WO$_3$ structures. Sol. Energy Mater. Sol. Cell. *136*, 86–91. https://doi.org/10.1016/j.solmat.2015.01.002.

175. Lin, Y.-S., Lai, Y.C., Tsai, T.H., Chen, P.C., and Liao, M.C. (2018). Flexible electrochromic tungsten/titanium mixed oxide films synthesized onto flexible polyethylene terephthalate/indium tin oxide substrates via low temperature plasma polymerization. Thin Solid Films *651*, 56–66. https://doi.org/10.1016/j.tsf.2018.01.039.

176. Wang, Y., Zhang, L., Cui, K., Xu, C., Li, H., Liu, H., and Yu, J. (2018). Solar driven electrochromic photoelectrochemical fuel cells for simultaneous energy conversion, storage and self-powered sensing. Nanoscale *10*, 3421–3428. https://doi.org/10.1039/c7nr09275j.

177. Li, N., Li, Y., Sun, G., Ma, Y., Chang, T., Ji, S., Yao, H., Cao, X., Bao, S., and Jin, P. (2017). Selective and Tunable Near-Infrared and Visible Light Transmittance of MoO(3-x) Nanocomposites with Different Crystallinity. Chem. Asian J. *12*, 1709–1714. https://doi.org/10.1002/asia.201700437.

178. Liang, X., Chen, M., Guo, S., Zhang, L., Li, F., and Yang, H. (2017). Dual-Band Modulation of Visible and Near-Infrared Light Transmittance in an All-Solution-Processed Hybrid Micro-Nano Composite Film. ACS Appl. Mater. Interfaces *9*, 40810–40819. https://doi.org/10.1021/acsami.7b11582.

179. Eric, H., Li, H., and Adulhakem Y, E. (2019). Rechargeable Zn(2+/)Al(3+) dual-ion electrochromic device with long life time utilizing dimethyl sulfoxide (DMSO)-nanocluster modified hydrogel electrolytes. RSC Adv. *9*, 32047–32057. https://doi.org/10.1039/c9ra06785j.

180. Zhang, S., Li, Y., Zhang, T., Cao, S., Yao, Q., Lin, H., Ye, H., Fisher, A., and Lee, J.Y. (2019). Dual-Band Electrochromic Devices with a Transparent Conductive Capacitive Charge-Balancing Anode. ACS Appl. Mater. Interfaces *11*, 48062–48070. https://doi.org/10.1021/acsami.9b17678.

181. Ling, H., Wu, J., Su, F., Tian, Y., and Liu, Y.J. (2021). Automatic light-adjusting electrochromic device powered by perovskite solar cell. Nat. Commun. *12*, 1010. https://doi.org/10.1038/s41467-021-21086-7.

182. Huang, Q., Wang, J., Gong, H., Zhang, Q., Wang, M., Wang, W., Nshimiyimana, J.P., and Diao, X. (2021). A rechargeable electrochromic energy storage device enabling effective energy recovery. J. Mater. Chem. A Mater. *9*, 6451–6459. https://doi.org/10.1039/d0ta11234h.

183. Guo, W., Cong, Z., Guo, Z.H., Zhang, P., Chen, Y., Hu, W., Wang, Z.L., and Pu, X. (2021). Multifunctional Self-Charging Electrochromic Supercapacitors Driven by Direct-Current Triboelectric Nanogenerators. Adv. Funct. Mater. *31*. https://doi.org/10.1002/adfm.202104348.

184. Cai, G., Darmawan, P., Cheng, X., and Lee, P.S. (2017). Inkjet Printed Large Area Multifunctional Smart Windows. Adv. Energy Mater. *7*. https://doi.org/10.1002/aenm.201602598.

185. Ma, D., and Wang, J. (2016). Inorganic electrochromic materials based on tungsten oxide and nickel oxide nanostructures. Sci. China Chem. *60*, 54–62. https://doi.org/10.1007/s11426-016-0307-x.

186. Alzahrani, J.S., Sharma, A., Nazrin, S.N., Alrowaili, Z.A., and Al-Buriahi, M.S. (2022). Optical and radiation shielding effectiveness of a newly fabricated WO3 doped TeO2–B2O3 glass system. Radiat. Phys. Chem. *193*, 109968. https://doi.org/10.1016/j.radphyschem.2022.109968.

187. Almuqrin, A.H., and Sayyed, M.I. (2021). Radiation shielding characterizations and investigation of TeO2–WO3–Bi2O3 and TeO2–WO3–PbO glasses. Appl. Phys. A *127*, 190. https://doi.org/10.1007/s00339-021-04344-9.

188. Stalin, S., Gaikwad, D.K., Al-Buriahi, M.S., Srinivasu, C., Ahmed, S.A., Tekin, H.O., and Rahman, S. (2021). Influence of Bi2O3/WO3 substitution on the optical, mechanical, chemical durability and gamma ray shielding properties of lithium-borate glasses. Ceram. Int. *47*, 5286–5299. https://doi.org/10.1016/j.ceramint.2020.10.109.

189. Hopmann, E., and Elezzabi, A.Y. (2020). Electrochemical Stability Enhancement of Electrochromic Tungsten Oxide by Self-Assembly of a Phosphonate Protection Layer. ACS Appl. Mater. Interfaces *12*, 1930–1936. https://doi.org/10.1021/acsami.9b19961.

190. Kim, J., Inamdar, A.I., Jo, Y., Cho, S., Aqueel Ahmed, A.T., Hou, B., Cha, S., Kim, T.G., Kim, H., Im, H., and Im, H. (2020). Nanofilament array embedded tungsten oxide for highly efficient electrochromic supercapacitor electrodes. J. Mater. Chem. A Mater. *8*, 13459–13469. https://doi.org/10.1039/d0ta01728k.

191. Chen, J., Wang, Z., Liu, C., Chen, Z., Tang, X., Wu, Q., Zhang, S., Song, G., Cong, S., Chen, Q., and Zhao, Z. (2021). Mimicking Nature's Butterflies: Electrochromic Devices with Dual-Sided Differential Colorations. Adv. Mater. *33*, e2007314. https://doi.org/10.1002/adma.202007314.

192. Chang, C.-M., Chiang, Y.-C., Cheng, M.-H., Lin, S.-H., Jian, W.B., Chen, J.-T., Cheng, Y.J., Ma, Y.-R., and Tsukagoshi, K. (2021). Fabrication of WO3 electrochromic devices using electro-exploding wire techniques and spray coating. Sol. Energy Mater. Sol. Cell. *223*, 110960. https://doi.org/10.1016/j.solmat.2021.110960.

193. Wang, S., Xu, H., Hao, T., Wang, P., Zhang, X., Zhang, H., Xue, J., Zhao, J., and Li, Y. (2021). In situ XRD and operando spectra-electrochemical investigation of tetragonal WO3-x nanowire networks for electrochromic supercapacitors. NPG Asia Mater. *13*, 51. https://doi.org/10.1038/s41427-021-00319-7.